TIME-RESOLVED VACUUM-ULTRAVIOLET PHOTOELECTRON SPECTROSCOPY OF THE $\tilde{A}\ ^1A_u$ STATE OF ACETYLENE

Weronika O. Razmus,[a#] Antonio Prlj,[b#] Nathan A. Seifert,[c] Matteo Bonanomi,[d] Carlo Callegari,[e] Miltcho Danailov,[e] Piero Decleva,[f] Alexander Demidovich,[e] Giovanni De Ninno,[e,g] Michele Devetta,[h] Davide Faccialà,[h] Raimund Feifel,[i] Luca Giannessi,[e,j] Tomislav Piteša,[b] Ivan Powis,[k] Lorenzo Raimondi,[e] Katharine L. Reid,[k] Primož Rebernik Ribič,[e,g] Carlo Spezzani,[e] Richard J. Squibb,[i] James O. F. Thompson,[k] Oksana Plekan,[e] Caterina Vozzi,[h] Emily M. Warne,[a] Marco Zangrando,[e,l] Kevin C. Prince,[e,m] Michele Di Fraia,[e] David M. P. Holland,[n] Russell S. Minns,[a] Nađa Došlić,[b] and Stephen T. Pratt,[o*]

a. University of Southampton, Chemistry Department, Southampton SO17 1BJ, Hants, England
b. Ruđer Bošković Institute, Department of Physical Chemistry, Bijenička 54 10000 Zagreb, Croatia
c. University of New Haven, Department of Chemistry and Chemical and Biomedical Engineering, 300 Boston Post Rd, West Haven, CT 06516 USA
d. Politecnico Milan, I-20133 Milan, Italy
e. Elettra Sincrotrone Trieste, I-34149 Trieste, Italy
f. University of Trieste, CNR IOM, Via Giorgieri 1, I-34127 Trieste, Italy
g. University of Nova Gorica, Vipavska 13, SI-5000 Nova Gorica, Slovenia
h. Consiglio Nazionale delle Ricerche (CNR), Istituto di Fotonica e Nanotecnologie, I-20133 Milan, Italy
i. University of Gothenburg, Origovägen 6B, 41258 Gothenburg, Sweden

j. INFN Laboratori Nazionali di Frascati, Via E. Fermi 54, 00044 Frascati (Roma)

k. Department of Chemistry, University of Nottingham, Nottingham NG7 2RD, England

l. CNR - Istituto Officina dei Materiali (IOM), I-34149 Trieste, Italy

m. Department of Chemistry and Biotechnology, School of Science, Computing and Engineering Technologies, Swinburne University of Technology, Melbourne, Victoria 3122, Australia

n. STFC, Daresbury Laboratory, Daresbury, Warrington, Cheshire, WA4 4AD, UK

o. Chemical Sciences and Engineering Division, Argonne National Laboratory, Lemont, IL 60439 USA

#Joint first authors
*Corresponding Author Email: stpratt@anl.gov

ABSTRACT

Ultrafast time-resolved photoelectron spectra are reported for the vacuum-ultraviolet (VUV) photoionization of acetylene following excitation to the $\widetilde{A}\ ^1A_u$ state via ultraviolet (UV) absorption at 200-nm. The excitation energy lies above the lowest dissociation threshold to C_2H $\widetilde{X}\ ^2\Sigma^+ + H$, as well as above the threshold for adiabatic dissociation of the $\widetilde{A}\ ^1A_u$ state to form C_2H $(\widetilde{A}\ ^2\Pi) + H$. The time-dependent mass spectra and photoelectron spectra provide insight into the intramolecular decay processes of the $\widetilde{A}\ ^1A_u$ state. In addition, photoelectron spectra of the $\widetilde{A}\ ^1A_u$ state with VUV light access both the $\widetilde{X}\ ^2\Pi_u$ and $\widetilde{A}\ ^2\Sigma_g^+$ states of the ion, as well as the predicted, but previously unobserved, $1\ ^2\Pi_g$ state, which corresponds to a two-hole, one-particle configuration that lies in close proximity to the $\widetilde{A}\ ^2\Sigma_g^+$ state. The $1\ ^2\Pi_g$ state is split into $^2A_2 + {}^2B_2$ and $^2A_g + {}^2B_g$ states in the *cis* and *trans* configurations, respectively. Electronic structure calculations, along with trajectory calculations, reproduce the principal features of the experimental data, and confirm the assignment of the $1\ ^2\Pi_g$ state.

Keywords: acetylene, time-resolved photoelectron spectroscopy, pump-probe, intramolecular dynamics

I. INTRODUCTION

Photoelectron spectroscopy of excited state molecules is a powerful tool to characterize the energetics and dynamics of both neutral and ionic states. In time-resolved photoelectron spectroscopy, the excited state of interest is prepared by a UV pump pulse and ionized by a delayed probe pulse to record the time-dependent photoelectron spectra.[1,2,3] These spectra reflect the evolving character of the excited level as projected onto the ionic states, and thus reflect the intramolecular dynamics of the excited state. When the probe photons are of relatively low energy, ionization usually occurs by photoionization out of the excited orbital populated by the pump pulse, resulting in single-hole valence states of the molecular cation. These valence states are those accessed in single-photon photoelectron spectroscopy of ground-state molecules.

In isolated molecules, intramolecular relaxation (internal conversion or intersystem crossing) of the pumped level can populate high vibrational levels of the lower-lying electronic states (including the ground electronic state), which require higher photon energies to access the full Franck-Condon envelope of the ionizing transition. Vacuum ultraviolet (VUV) probe pulses for time-resolved photoelectron spectroscopy have been generated by using both high-harmonic generation[4,5] and free-electron laser sources.[6,7,8] The use of higher energy probe photons also introduces the possibility of ionization from more strongly bound orbitals of the molecule, and for accessing new excited states of the ion. Higher energy X-ray sources have also been used as probes in time-resolved photoelectron spectroscopy to allow site-specific inner-shell excitation to follow the evolution of the pump-initiated process.[9,10]

In the present work, we use time-resolved photoelectron spectroscopy with a VUV probe to study the intramolecular relaxation and photoionization dynamics of the $\widetilde{A}\ ^1A_u$ state of acetylene. The spectroscopy and dynamics of the $\widetilde{A}\ ^1A_u$ state of acetylene have been the subject of intense experimental and theoretical studies for decades.[11,12,13,14,15,16,17,18,19,20,21,22,23,24,25,26,27,28,29] Photoexcitation from the linear $\widetilde{X}\ ^1\Sigma_g^+$ state, with dominant configuration $\ldots(3\sigma_g)^2(1\pi_u)^4$, to the

trans-bent $\tilde{A}\ ^1A_u$ state involves a π to π* transition and results in a long progression in the ν_3' *trans*-bending vibration.[11,12,14] Intramolecular relaxation of the $\tilde{A}\ ^1A_u$ state involves coupling with several triplet states, internal conversion to the ground state, possible isomerization to the CCH_2 vinylidene structure, and dissociation to C_2H + H. A schematic energy level diagram is given in Figure 1, and the relevant energetics are given in Table I.

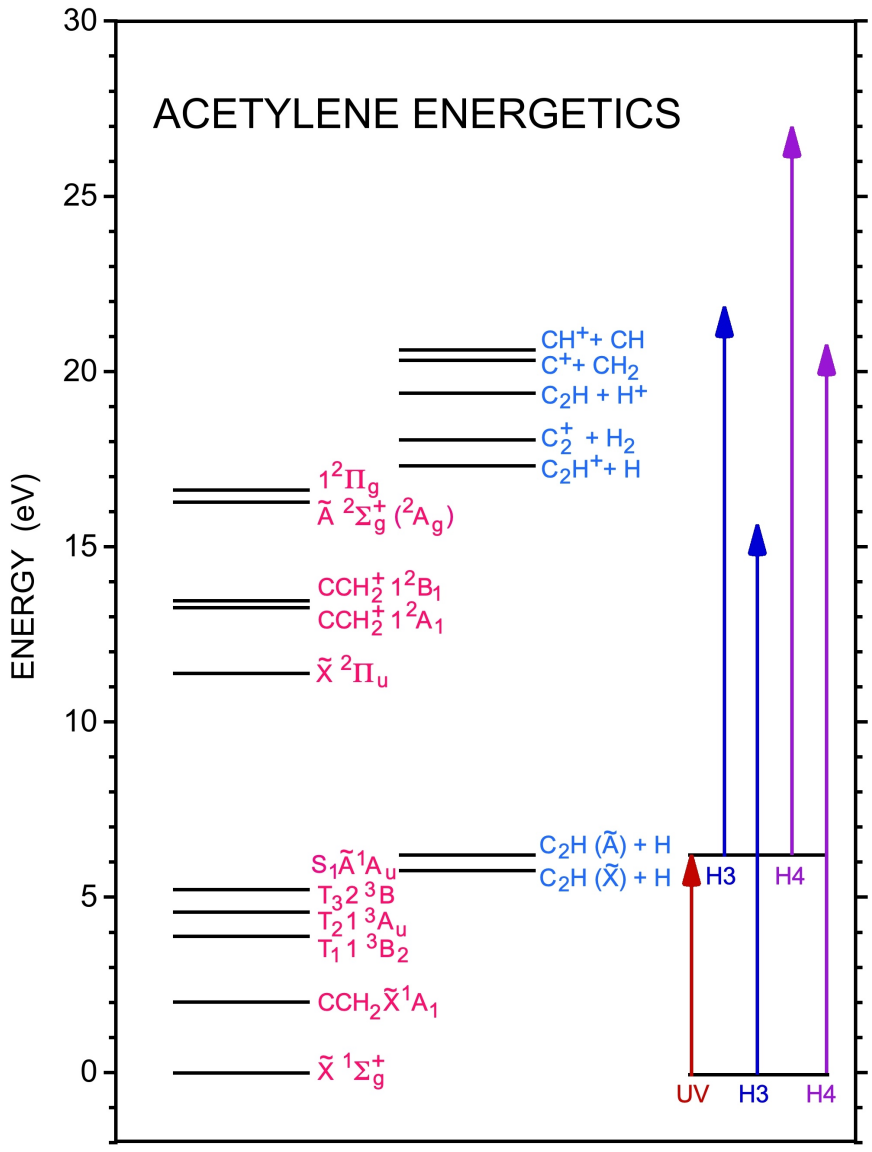

Figure 1. A schematic energy level diagram with the relevant levels for C_2H_2 and $C_2H_2^+$. The energies and their sources are provided in Table 1.

Table 1. Some Relevant Energies for Acetylene and Its Isomers.[a]

Level	Energy (eV)
HCCH $\tilde{X}\ ^1\Sigma_g^+$	0.0
CCH_2 $\tilde{X}\ ^1A_1$	2.020[b]
HCCH T_1 1 $^3B_2$	3.89[c]
HCCH T_2 1 ^3A_u	4.57[c]
HCCH T_3 2 ^3B	5.1900[d]
HCCH $\tilde{A}\ ^1A_u$	5.2318[e]
C_2H ($\tilde{X}\ ^2\Sigma^+$) + H	5.712 ± 0.001[f]
C_2H ($\tilde{A}\ ^2\Pi$) + H	6.170 ± 0.001[f,g]
$HCCH^+$ $\tilde{X}\ ^2\Pi_u$	11.40078 ± 0.00006[h]
$HCCH^+$ 1 $^2\Pi_g$	16.640[b,h,i]
$HCCH^+$ $\tilde{A}\ ^2A_u$	16.297 ± 0.005[j]
CCH_2^+ 1 $^2A_1$	13.292[b]
CCH_2^+ 1 $^2B_1$	13.444[b]
C_2H^+ + H	17.358 ± 0.001[k]
C_2^+ + H_2	18.067 ± 0.004[k]
C_2H + H^+	19.377 ± 0.001[k]
C^+ + CH_2	20.314 ± 0.003[k]
CH^+ + CH	20.635 ± 0.001[k]
Third Harmonic VUV	15.628
Fourth Harmonic VUV	20.838
200 nm Photon	6.199

(a) The values represent the energies at the equilibrium geometries/stationary points of the different species.
(b) Reference 42.
(c) Reference 29.
(d) Reference 16.
(e) Origin band, Reference 14.
(f) Reference 18.
(g) Reference 31.
(h) Reference 53.
(i) In Reference 42, the 1 $^2\Pi_g$ state in the linear geometry is calculated to lie 0.140 eV below the $\tilde{A}\ ^2A_u$ state in its linear geometry, or 5.239 eV above the $\tilde{X}\ ^2\Pi_u$ state. The relative energies of the $\tilde{A}\ ^2A_g$ and 1 $^2\Pi_g$ states vary with geometry, but assuming the separation is constant, the bent components of the 1 $^2\Pi_g$ state should lie at approximately 16.157 eV.
(j) Reference 35.
(k) Reference 30.

For the present study, high vibrational levels of the $\widetilde{A}\ ^1A_u$ state are excited at 200 nm (6.199 eV) in a region that has been characterized by Van Craen et al.[13] This energy lies well above the dissociation threshold to C_2H ($\widetilde{X}\ ^2\Sigma^+$) + H ground state products (5.7097 ± 0.0011 eV),[30] and just above the threshold for adiabatic dissociation to C_2H ($\widetilde{A}\ ^2\Pi$) + H (6.1675 ± 0.0011 eV).[30,31] Calculations by Cui and Morokuma[28] provided a path from the initially excited S_1 ($\widetilde{A}\ ^1A_u$) state through a sequence of triplet states $S_1 \rightarrow T_3 \rightarrow T_2 \rightarrow T_1$ that ultimately leads to C_2H ($\widetilde{X}\ ^2\Sigma^+$) + H. At energies near the dissociation threshold, both experiment and theory indicate the timescale for the intersystem crossing step is ~100 ps. More recent experiments by Yamakita et al.[32] focused on energies around the adiabatic dissociation threshold for C_2H ($\widetilde{A}\ ^2\Pi$) + H, and they found the lifetime decreased from ~100 ps near 5.827 eV to ~25 ps at 6.274 eV. The 25 ps lifetime is still longer than the C_2H_2 rotational period, and thus still allows rotational resolution in the absorption spectrum. From their jet-cooled absorption spectra, Yamakita et al.[32] assigned the rotational structure in five vibronic bands between 6.197 eV and 6.204 eV, although detailed vibrational assignments were not possible for all of these. Note that in addition to the resolved rotational structure, the room-temperature spectrum of Van Craen et al.[13] also appears to show weak continuous absorption, indicating some of the relaxation is faster than 25 ps.

In the present experiment, the FERMI free-electron laser[33] operating between 15 and 21 eV is used to probe the excited state dynamics and a magnetic bottle electron spectrometer[8] is used to record the time-resolved photoelectron spectrum. In principle, this arrangement allows the observation of dynamics on the S_1 and S_0 surfaces, on the T_1, T_2, and T_3 surfaces, and on surfaces associated with the vinylidene structure or other isomeric forms of acetylene. The experimental results are complemented by theoretical results on the photoionization and photodissociation of the $\widetilde{A}\ ^1A_u$ state that were obtained by using mixed quantum-classical trajectories on the excited state surface.

Traditional photoelectron spectroscopy from the ground state of acetylene shows strong bands corresponding to the production of the $\widetilde{X}\ ^2\Pi_u$ and $\widetilde{A}\ ^2\Sigma_g^+$ states of the cation.[34,35] These processes

correspond to ionization out of the $1\pi_u$ highest occupied molecular orbital (HOMO) and the $3\sigma_g$ (HOMO-1). The $\tilde{A}\ ^1A_u$ state has the dominant configuration $\ldots(3\sigma_g)^2(1\pi_u)^3(1\pi_g)^1$, and photoionization from this state has several intriguing features. Earlier two-photon photoelectron spectroscopy via the $\tilde{A}\ ^1A_u$ state was performed with photon energies that only allowed access to the $\tilde{X}\ ^2\Pi_u$ of the ion.[36,37] Interestingly, theoretical calculations indicate that the $1\ ^2\Pi_g$ state of the cation lies very close to the $\tilde{A}\ ^2\Sigma_g^+$ state,[38,39,40,41,42] but it has not been observed experimentally.[35] The $1\ ^2\Pi_g$ state is a two-hole, one-particle state with the dominant configuration $\ldots(3\sigma_g)^2(1\pi_u)^2(1\pi_g)^1$, i.e., two holes in the $1\pi_u$ HOMO and one electron in the excited $1\pi_g$ LUMO. Thus, the $1\ ^2\Pi_g$ state cannot be reached in a dipole-allowed single-photon transition from the $\tilde{X}\ ^1\Sigma_g^+$ ground state, although Cederbaum et al.[39] have predicted a very weak transition resulting from configuration interaction. This $1\ ^2\Pi_g$ state splits into two more stable components with $^2A_2 + {}^2B_2$ and $^2A_g + {}^2B_g$ symmetry in the *cis* and *trans* geometries, respectively. Interestingly, VUV photoionization of the $\tilde{A}\ ^1A_u$ state that removes a second $1\pi_u$ electron instead of the $1\pi_g$ electron leads directly to the two-hole, one-particle $1\ ^2\Pi_g$ state. Indeed, this transition from the $\tilde{A}\ ^1A_u$ state is expected to be considerably stronger than the transition from the $\tilde{A}\ ^1A_u$ state to the $\tilde{A}\ ^2\Sigma_g^+$ continuum, which has the dominant configuration $\ldots(3\sigma_g)^1(1\pi_u)^4(1\pi_g)^0$, and thus requires a two-electron process that is expected to be very weak. Two-hole, one-particle states like $C_2H_2^+\ 1\ ^2\Pi_g$ are often populated in resonant Auger decay via spectator decay processes,[43,44] and the ability to access such states directly may considerably enhance the ability to assign them more rigorously.

II. METHODS

A. Experiment

The present pump-probe study was performed using FEL-1 at the FERMI Free-Electron Laser Facility.[45] Many details of the experiment have been described previously, and they are discussed only briefly here.[46,47,48,49] Experiments with the seeded FEL were performed at a repetition rate of 50 Hz with either the third (H3) or fourth (H4) harmonic of the 238-nm seed laser, corresponding

to vacuum ultraviolet (VUV) wavelengths (photon energies) of 79.33 nm (15.628 eV) and 59.50 nm (20.838 eV), respectively. We present the data associated with the fourth harmonic, H4, in this paper and the supporting measurements with the third harmonic, H3, in the Supplemental Material.[50] The FEL, beam delivery system, pump laser, and optical arrangement for the pump-probe experiment have already been described.[8,45,46,47,48] The electron kinetic energy measurements were performed using the magnetic bottle electron spectrometer at the Low-Density Matter End Station, which has also been described previously.[8] Mass spectra were also recorded using the same setup with the potentials switched for the detection of ions. A slight misalignment of the apparatus resulted in mass peaks with two weaker asymmetric side bands, but this did not affect the interpretation of the present results.

The duration of the FEL seed pulse was determined to be 125 fs FWHM before the experiment began, resulting in estimated VUV pulse durations of 86 ± 14 fs and 77 ± 15 fs for H3 and H4, respectively. The bandwidth was measured on a shot-by-shot basis by using the PADRES spectrometer,[51] and was typically 10^{-3} of the VUV wavelength. This value corresponds to a bandwidth of 0.016 eV and 0.021 eV for H3 and H4 respectively. The VUV output from the FEL was circularly polarized. The VUV pulse energy out of the FEL was typically 25 μJ and 40 μJ for H3 and H4, respectively, and after transport losses was ~5 μJ in the interaction region. The VUV beam was focused to a 30 x 30 μm^2 spot.

The pulse duration of the 200-nm UV pump pulse was estimated to be 200 – 250 fs, with a bandwidth of 0.6 nm (0.019 eV). The UV pulse energy was also typically ~5 μJ in the interaction region, and this could be reduced by a polarizer and half-wave plate combination. The UV pump was focused to a 150 μm diameter spot to overlap the FEL probe pulse. The UV light was linearly polarized in the plane perpendicular to the flight tube axis. A delay stage for the pump beam allowed for a range of delays from negative values (VUV probe pulse before the UV pump pulse) to positive values (VUV probe pulse after the UV pump pulse) up to 600 ps. The sample gas was

5% acetylene in He at a pressure of 1-2 bar, which was introduced into the interaction region via a pulsed valve (Parker Hannifin) with a 100 μm diameter nozzle.

The sample rotational temperature was not measured directly but based on previous measurements, it is expected to be 10 – 20 K. The valve timing was synchronized with the arrival of the pump pulse. For some of the spectra, background data were recorded with the valve firing out of sync every third FEL pulse. The photoelectron spectra were calibrated by using well-known spectra of rare gases[52] (Kr and Xe) and acetylene[35,53] recorded with the FEL alone. Additional calibration points came from the ionization of He[52] via a two-photon process, and from the ionization of a small acetone[54] impurity in the acetylene sample. The electric field in the interaction region of the spectrometer is ~10.5 V/cm, which shifts the measured ionization energy by ~0.002 eV.

B. Computational Methods

The theoretical effort involved a combination of electronic structure calculations for the relevant states of C_2H_2 and $C_2H_2^+$, trajectory calculation for the dynamics on the relevant surfaces, and the simulation of the time-dependent photoelectron spectra.

For the electronic structure calculations, we employ extended multi-state complete active space second order perturbation theory (XMS-CASPT2),[55] as implemented in the Bagel program package.[56] The active space was composed of 8 electrons in 8 orbitals - two pairs of π and π* orbitals, and two pairs of bonding σ and antibonding σ* orbitals, as shown in Figure 2.

To calculate the XMS-CASPT2 electronic states of the neutral system, we used state-averaged complete active space self-consistent field (SA-CASSCF) wavefunctions with 4 singlet states in state-averaging, namely the SA(4)-CASSCF(8,8). For the cationic states, we performed calculations using state-averaging with 7 states. All calculations were performed with the diffuse def2-SVPD basis set.[57] XMS-CASPT2 calculations were performed with the frozen core and

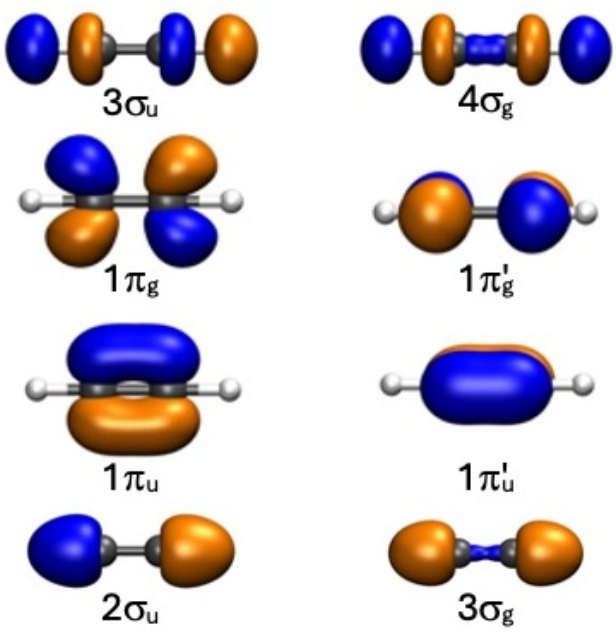

Figure 2. The eight orbitals making up the active space for the present calculations, including two pairs of π and π * orbitals, and two pairs of σ and σ* orbitals.

density-fitting approximations, using a single state - single reference (SS-SR) contraction scheme,[58,59] and with real vertical shift values set to 0.5 a.u. to avoid problems with intruder states.

The first part of the reaction path was constructed by linear interpolation in internal coordinates between the ground state minimum (Franck-Condon geometry) and the global minimum of the S_1 $\tilde{A}$ ^1A_u state with *trans* geometry. The second part was obtained by linear interpolation between the Franck-Condon geometry and the local minimum of the S_1 state with *cis* geometry ($^1A_2$). Figure 3 shows the two parts linked together. In total, the *trans* and *cis* S_1 minima were connected by 19 geometry points. In addition, rigid scans of hydrogen dissociation from both *cis* and *trans* minima were performed in steps of 0.1 Å.

The valence time-resolved photoelectron spectrum was simulated using the classical limit of the doorway-window formalism.[60,61,62,63] The procedure, which is described in more detail in the Supplemental Material,[50] is carried out in three steps. The first step involves the evaluation of the classical doorway function, that is, the geometries and momenta from the ground state Wigner distribution are sampled by taking into account the carrier frequency and shape of the pump pulse and the oscillator strength of the electronic transition. The second step involved the promotion of the ground state ensemble to the excited state manifold and the propagation of nonadiabatic trajectories. Nonadiabatic dynamics simulations were performed with Tully's fewest switches

surface hopping (FSSH)[64] algorithm using an in-house code coupled to the BAGEL electronic structure calculations.[56,65] The third step involved the evaluation of the classical window function describing the photoionization of the excited state ensemble.

The theoretical assignment of the time-resolved signal was obtained by diabatization of the cationic states.[66,67] Details of the diabatization procedure are given in the Supplemental Material.[50] The results of the assignment, i.e., how the theoretical photoelectron intensity is allocated to different diabatic states of the ion, are shown in Figure S1.

III. RESULTS AND DISCUSSION

A. Theoretical Overview

Figure 3 shows the variation of the potential energies of the neutral molecule in the S_0 ($\tilde{X}\ ^1\Sigma_g^+$), S_1, and S_2 states, and the cation in the D_0 – D_4 states, along the isomerization reaction path encompassing the S_1 *trans* minimum with geometry (C-H distance 1.107 Å), the linear Franck-Condon geometry (C-H distance 1.077 Å), the S_1 *cis* minimum (C-H distance 1.111 Å), and the subsequent C-H dissociation path. Specifically, the curves follow the isomerization coordinate between the linear geometry and the *trans* and *cis* equilibrium geometries, at which points the angles are fixed and one of the C-H bonds is extended towards dissociation to C_2H + H (or C_2H^+ + H). The shapes of the curves for the neutral and ion states are generally in good agreement with the results of Perić et al.[68,69] Although the output of the calculation gives adiabatic states in order of increasing energy, the ion states in Figure 3 have been drawn to show the quasi-diabatic states that were extracted by preserving the continuity of the Dyson norms as a function of geometry. The potential energy profiles indicate that after excitation to the S_1 state, the system rapidly relaxes either towards the *trans* or the *cis* minimum, and that C-H dissociation is possible in the S_1 state because the kinetic energy that the system gains when moving away from the Franck-Condon geometry to one of the minima is larger than the dissociation barrier. One can also see that, apart

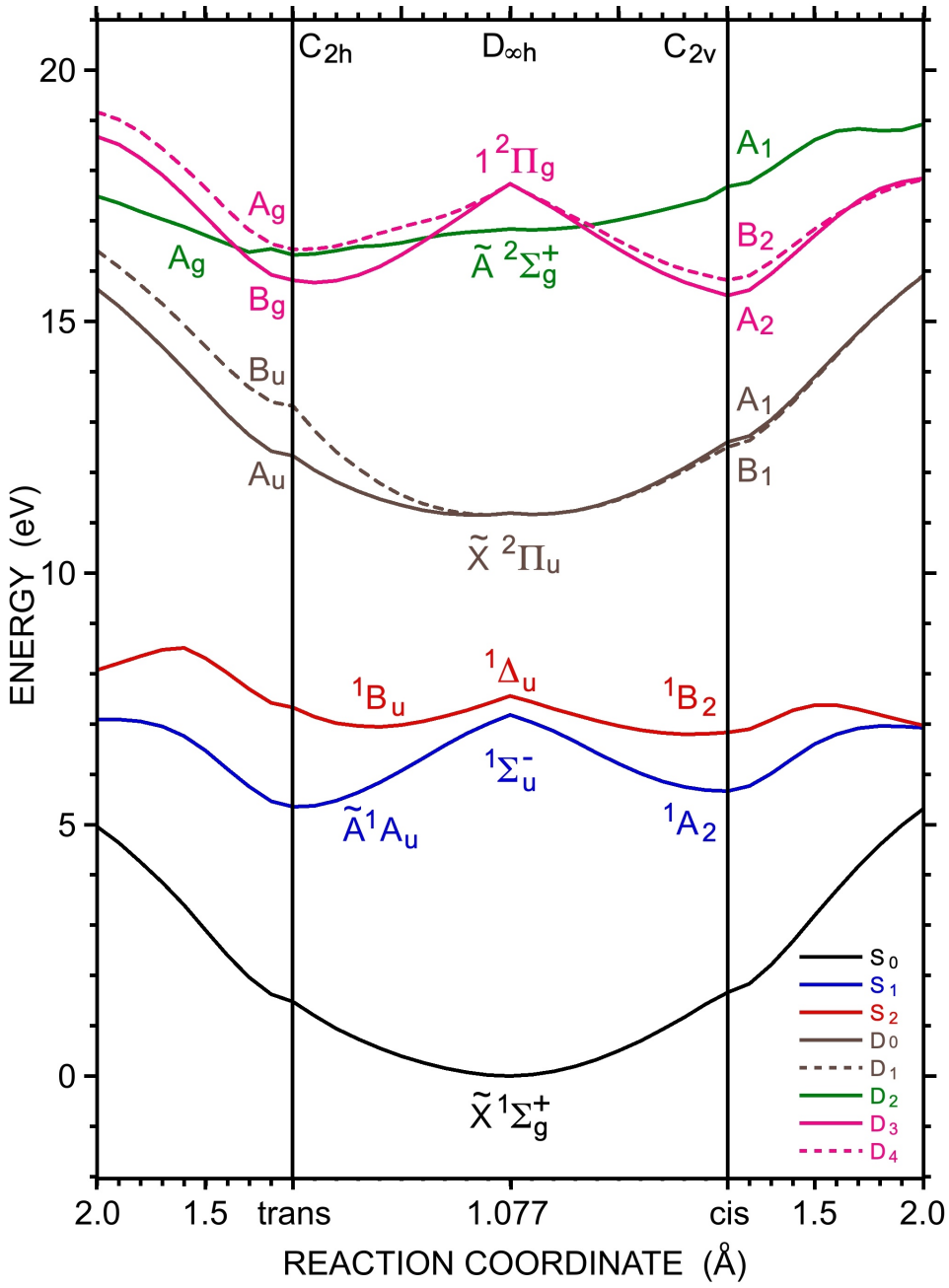

Figure 3. Potential energy curves for some electronic states of C_2H_2 and $C_2H_2^+$. The linear equilibrium geometry of the ground state neutral is in the center, with a C-H bond length of 1.077 Å. The x-axis is denoted the Reaction Coordinate, with the distance being the C-H bond length. To the left (right) the curves follow the potentials along the *trans* (*cis*) bending coordinate to the corresponding bent geometry, at which point the angles are fixed and one C-H bond is extended. The S_2 state is the lower Renner-Teller component of a linear $^1\Delta_u$ state. The Π states split in the nonlinear geometries, and the upper component is shown as a dashed line. The curves are plotted for the diabatic states obtained to preserve the smooth behavior of the Dyson norms through the curve crossings.

from the region in the *cis* geometry near the C-H dissociation limit, the S_1 and S_2 states are well separated along the whole reaction path. Specifically, the S_1 and S_2 states are separated by 1.97 and 1.16 eV at the geometries of the *trans* and *cis* minima, respectively. The two lowest electronic states of the cation, D_0 and D_1 correspond to the two components ($^2B_{3u}$ and $^2B_{2u}$, respectively, in the D_{2h} symmetry of the calculation) of the $\widetilde{X}\ ^2\Pi_u$ ground state and are found 11.20 eV above the electronic ground state at the equilibrium geometry of the ground state neutral. The D_2 state corresponds to the $\widetilde{A}\ ^2\Sigma_g^+$ state (^2A_g in the *trans* bent geometry) and the D_3 and D_4 states correspond to the two components (^2B_g and ^2A_g in the *trans* bent geometry) of the $1\ ^2\Pi_g$ state.[40,41,42] The latter three states remain in close proximity to each other over a wide range of geometries, including the *cis*- and *trans*-bent geometries. The $^4\Pi_g$ state based on the $\ldots(3\sigma_g)^2(1\pi_u)^2(1\pi_g)^1$ configuration is also expected at somewhat lower energy than the $1\ ^2\Pi_g$ and $\widetilde{A}\ ^2\Sigma_g^+$ states.[40,41,42] However, given the singlet character and small spin-orbit interactions of the $\widetilde{A}\ ^1A_u$ intermediate state, the transition to the triplet continuum associated with the quartet cation state is expected to be weak.[32]

The XMS(4)-CASPT2(8,8)/def2-SVPD vertical excitation energies of the three lowest singlet excited states of C_2H_2 are collected in Table S1 of the Supplemental Material.[50] The S_1 ($\widetilde{A}\ ^1A_u$) state, S_2 (^1B_u), and S_3 (^1A_u) states all correspond to $\pi\pi^*$ excitations. The S_1 state is found 7.18 eV above the ground state, while the degenerate S_2 and S_3 states are at 7.56 eV in the linear geometry. Geometry optimization of the S_1 state leads to a minimum with *trans* geometry 5.35 eV above the ground state. The S_2 and S_3 states are split by ~1.5 eV in the *trans* geometry and are found at 7.32 and 8.86 eV, respectively. It is also useful to consider the states near the H dissociation limit (d(C-H) = 3.0 Å). As expected, extension of the C-H bond increases the potential energy in the ground state and decreases the potential energy in the lowest $\pi\sigma^*$ state.

Figure 4 shows an expanded portion of Figure 3 that includes the five ion curves, along with the ionization intensity which was computed as the square of the Dyson norms. In the linear geometry, the next state at higher energy ($1\ ^2\Phi_g$) lies approximately 0.9 eV above the $1\ ^2\Pi_g$ state.[69] The length

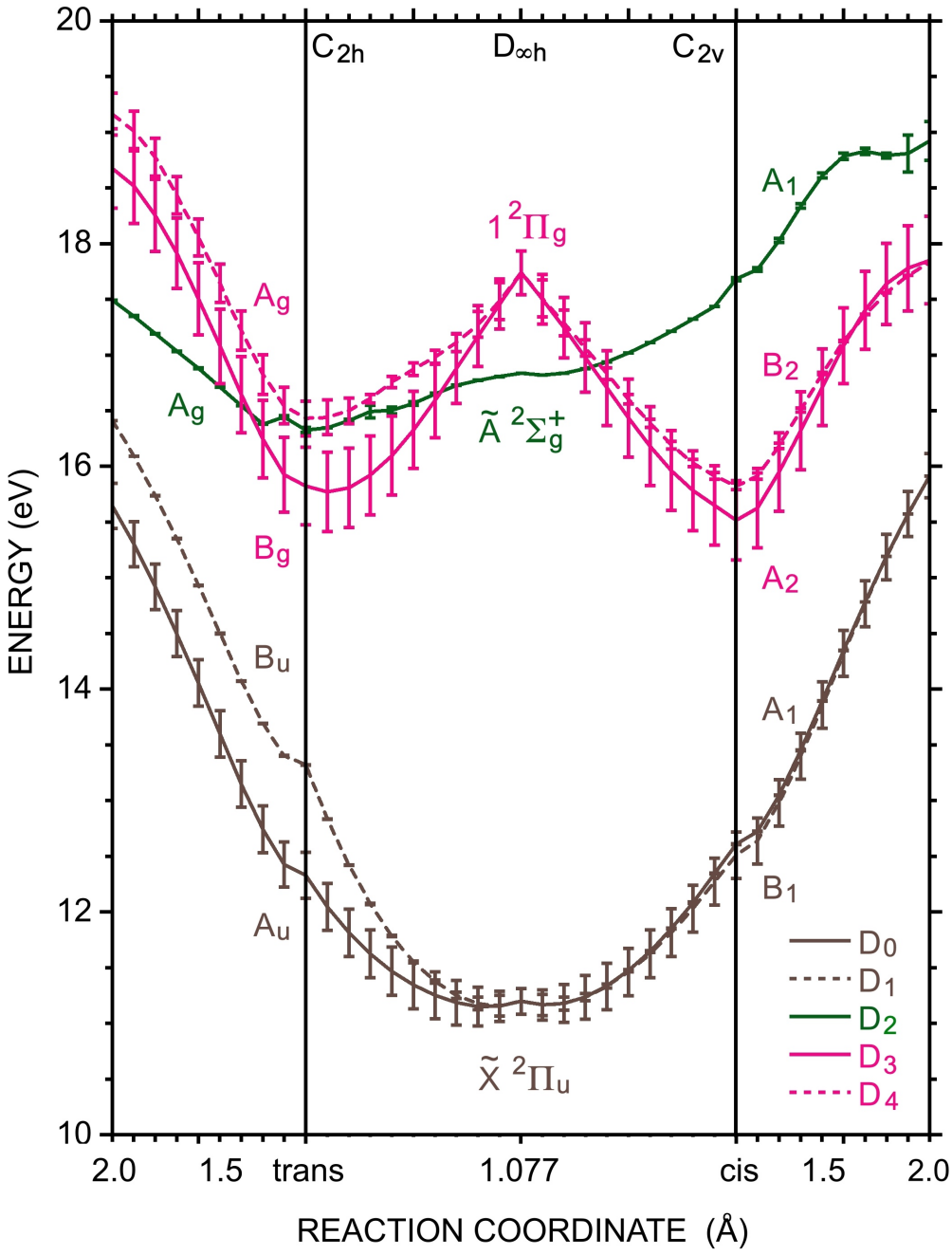

Figure 4. The potential curves for the first five ionic states of $C_2H_2^+$. See the caption of Figure 3 for details on the axes and labeling. The vertical lines at each point are equal to the square of the Dyson norms between the $\tilde{A}\ ^1A_u$ (S_1) state and the corresponding states of the ion. Diabatic states are drawn to preserve the smooth behavior of the Dyson norms through the curve crossings.

of the vertical lines at each point on the curves corresponds to the square of the Dyson norm from the S_1 state. The relaxation from the Franck-Condon geometry toward either the *trans* or the *cis*

minimum results in a rapid change in the binding energy of the S_1 state relative to the D_0 and D_1 states.

The trajectories in the $\tilde{A}\ ^1A_u$ state were propagated for up to 1 ps or until the molecule dissociated. Two aspects of these calculations deserve mention. First, on the timescale of the simulations (i.e., 1 ps), the trajectories remain primarily on the S_1 surface, with some excursions to the S_2 surface. There is some dissociation, with approximately 16% of the trajectories leading to C_2H + H. The dissociating trajectories are terminated, and the spectra of the C_2H and H fragments were not calculated. Second, analysis of the trajectories also shows significant rotation of the dihedral angle, τ, of the acetylene, leading to the conversion between the *trans*-bent and *cis*-bent structures. A histogram of the trajectories that shows how they sample the *trans*-bent and *cis*-bent structures in the $\tilde{A}\ ^1A_u$ (S_1) state is shown in Figure 5. In principle, TR-PES are expected to show the effects of both the *trans*- and *cis*- bent intermediate state structures. Note, however, that "*trans*" and "*cis*" in the figure do not necessarily denote the fully bent structures, but rather any CCH bending angle within the specified range of the dihedral angle. Thus, even nearly linear geometries are classified as *trans* and *cis*. Note also that the classical trajectories do not necessarily reflect the quantum behavior if the excitation process

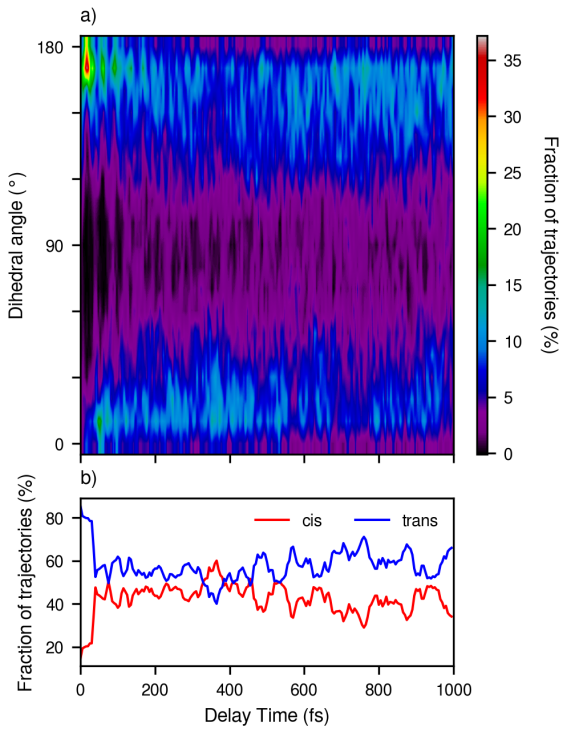

Figure 5. a) Two-dimensional histogram of nonadiabatic trajectories per time and the absolute value of the H-C-C-H dihedral angle, τ, normalized to the number of trajectories in each time to account for dissociating trajectories. b) The histogram from panel a) summed along the dihedral axis through the two intervals separately (cis: τ = 0-90°, trans: τ = 90-180°).

accesses single vibrational levels of the intermediate state but, in the present case, the pump spans multiple vibronic levels and the energy is above the adiabatic dissociation threshold.

B. Mass Spectra

Figure 6a shows the UV + VUV mass spectrum when the two pulses are overlapped in time. The spectra were recorded with the VUV light at 20.838 eV. The difference between the VUV_{only} and UV + VUV spectra is ~1-2% and not visible on the scale of the figure. The principal mass peaks arising from acetylene correspond to $C_2H_2^+$, C_2H^+, C_2^+, CH^+, C^+, and H^+ at masses of 26, 25, 24, 13, 12, and 1, respectively. Dissociative ionization by the 20.838 eV VUV pulse alone can account for these masses, with the parent ion and the C_2H^+ being the most important species.[70]

Figure 6b, c, and d show the difference spectra [(VUV+UV) – (VUV_{only})] with the VUV pulse before, overlapped with,

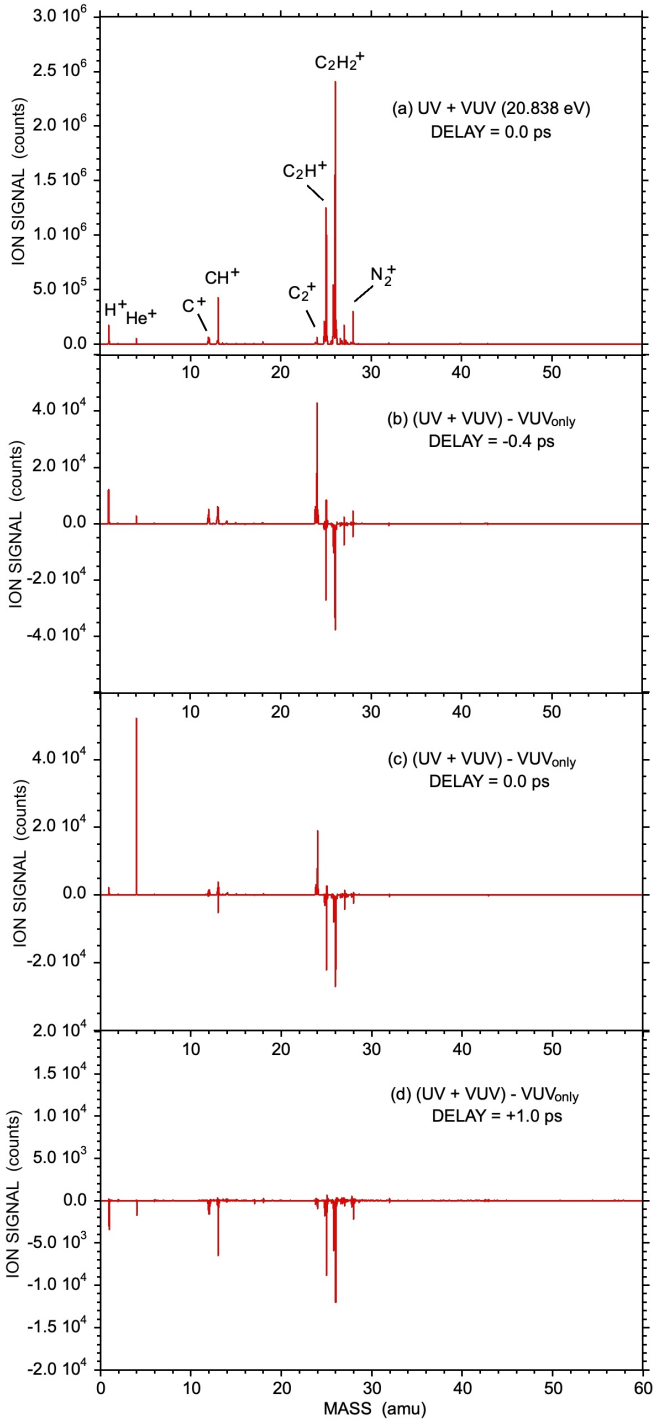

Figure 6. Mass spectra for the pump-probe experiments. (a) The total UV + VUV signal for a delay of 0.0 ps. (b) The (UV + VUV) – VUV_{only} difference signal for a delay of -0.4 ps. (c) Same as (b), but with a 0.0 ps delay. (d) Same as (b), but with a 1.0 ps delay.

and after the UV pulse, respectively. (The VUV pulse before the UV pulse corresponds to a negative delay.) For the spectra with the VUV pulse before or overlapped with the UV pulse, the UV pulse leads to a depletion in the $C_2H_2^+$ and C_2H^+ signals, with increases in the C_2^+, CH^+, C^+, and H^+ signals. These changes are attributed to photodissociation by the UV pulse of the $C_2H_2^+$ and C_2H^+ produced by the VUV pulse.

In contrast, when the UV pulse precedes the VUV pulse, the effect on the mass spectrum is smaller, with the difference peaks only a fraction of a percent of the size of the mass peaks. This effect seems to vary between small positive and small negative difference signals at each of the masses, with no consistent change in the signal as a function of delay time. This observation suggests that most of the signal arises from small errors in the subtraction process. Figure 6d shows a representative timepoint where there is depletion not only in the $C_2H_2^+$ and C_2H^+ signals, but also in the CH^+, C^+, and H^+ signals. This result may be due to the photodissociation of neutral C_2H_2 to produce neutral fragments in states for which the photoionization cross section is smaller than it is for the parent species.

As mentioned above, the mass spectra show small signals for several impurities. For example, a small signal is observed for acetone at mass 58, and for its dissociative ionization fragment, CH_3CO^+, at mass 43. Note that when the UV is before the VUV pulse, the UV can photodissociate the acetone to neutral fragments. As a result, the corresponding acetone photoelectron signal is bigger in the VUV_{only} spectrum than in the UV + VUV spectrum. This situation results in a negative going peak in the difference photoelectron spectra discussed in Section III.C. Similarly, very small signals are observed for N_2^+, O_2^+, and CO_2^+ at mass 28, 32, and 44, respectively.

The He carrier gas also produces a signal in the mass spectra. The strongest He^+ signal is observed when the VUV and UV pulses are overlapped in time (Figure 6c), indicating that it is produced by a two-color, two-photon process. The He^+ signal is small when the UV arrives before the VUV

pulse, and this very small residual signal is likely produced by the second harmonic of the VUV light. In contrast, the He^+ signal is significantly larger when the VUV pulse precedes the UV light by ~100 fs, suggesting that the UV and VUV are still partially overlapped at this delay. In Section III.D, the photoelectrons from this two-color, two-photon ionization of He are used to measure the cross correlation/instrument response time of the VUV and UV pulses.

C. Photoelectron Spectra

Figure 7 shows a contour plot of the difference spectrum of the UV + VUV and VUV-only photoelectron spectra obtained using the FEL fourth harmonic at 20.838 eV. The x-axis shows the electron kinetic energy in eV. The y-axis shows the delay of the VUV probe pulse relative to the UV pump pulse, and it has been split into a linear-time section at short delays and a log-time

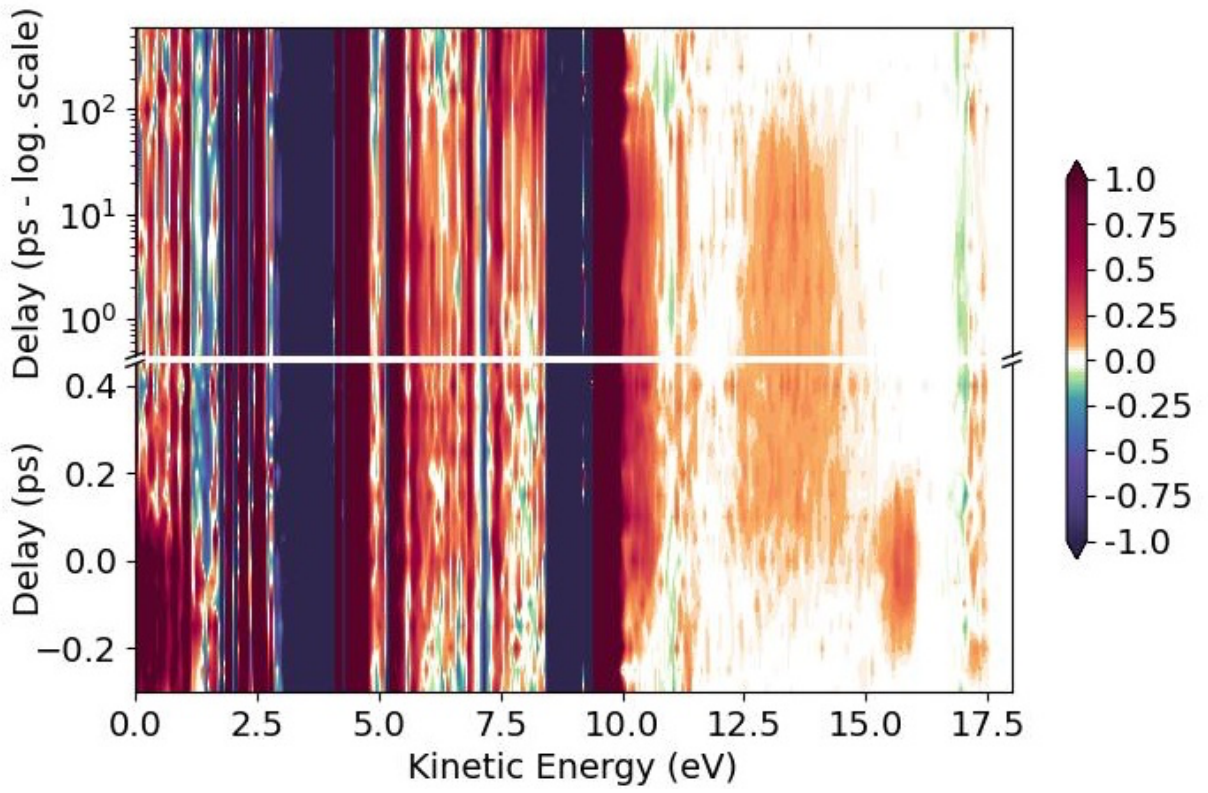

Figure 7. A contour plot of the photoelectron intensities following UV + VUV ionization of C_2H_2 as a function of time delay and electron kinetic energy for the pumped level ($\tilde{A}\ ^1A_u$ excited at 6.199 eV). The VUV probe corresponds to the fourth harmonic of the FEL at 20.838 eV.

section at long delays. Both the UV + VUV and VUV-only photoelectron spectra show extremely strong features resulting from the single-VUV-photon ionization of acetylene via the $\tilde{X}\ ^2\Pi_u \leftarrow X\ ^1\Sigma_g^+$ and $\tilde{A}\ ^2\Sigma_g^+ \leftarrow \tilde{X}\ ^1\Sigma_g^+$ transitions. The photoelectron spectrum recorded with VUV (20.838 eV) light alone is shown in Figure 8. For reference, the peak of the $\tilde{X}\ ^2\Pi_u$ band in Figure 8 is approximately $4x10^9$ counts, and the imperfect subtraction of the UV + VUV and VUV_{only} spectra, which may be due to a slight jitter in the timing for the two spectra, leads to a difference signal (i.e., Figure 7) for the corresponding peak of ~$5x10^7$ counts. In contrast, the difference signal for the peaks that can be unambiguously assigned to the UV + VUV process typically yield ~$5x10^5$ counts.

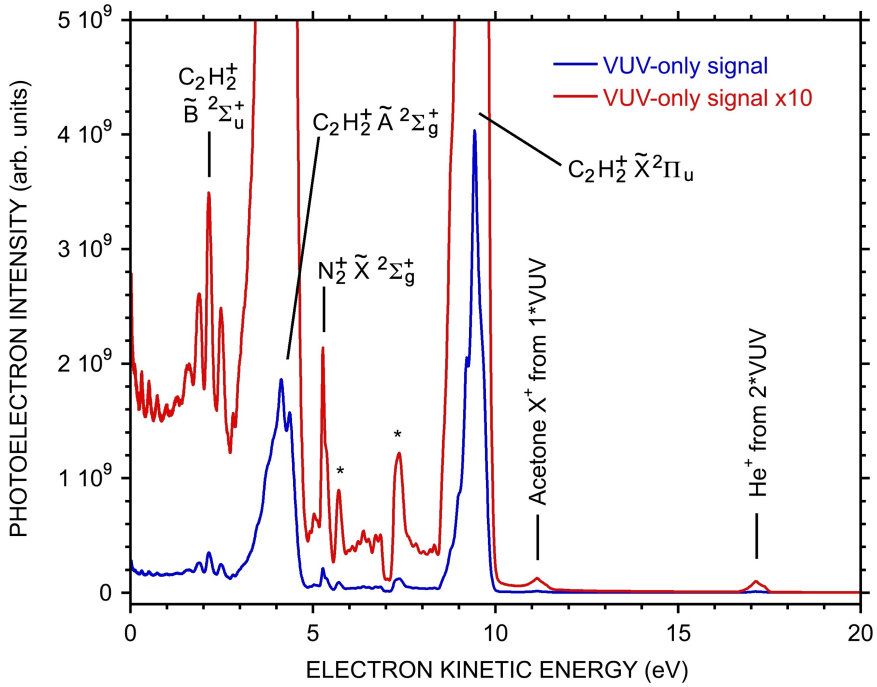

Figure 8. The VUV-only photoelectron spectrum of acetylene recorded at hν = 20.838 eV. The acetylene bands are indicated, along with signal from other species. Features labeled with * are believed to arise from ringing in the detection system from the intense $\tilde{X}\ ^2\Pi_u$ feature. The He^+ signal may arise from ionization by two VUV photons or by the second harmonic of the VUV light.

The large amplitude of the single-photon signals makes the analysis of features at kinetic energies below 9.4 eV (i.e., binding energies above 11.4 eV) difficult. Three VUV + UV features are

observed with kinetic energy below 9.4 eV. Although it is difficult to see in Figure 7, a feature at ~2.4 eV is assigned to the VUV + UV two-photon ionization of He and, as discussed in more detail below, can be used to characterize the instrument response function for the experiment. (Note that two-VUV-photon ionization produces a second He feature at a kinetic energy of ~17.1 eV in Figure 7.) The two additional features are observed at 7.5 – 8.2 eV and 5.6 – 7.0 eV, and they relate to dynamics of the acetylene molecule. These two features are also discussed in more detail below.

We now focus on electron kinetic energies above 9.4 eV. Figure 9a shows the time-dependent contour plot for this energy range obtained with the FEL energy of 20.838 eV. The corresponding plot with the FEL energy of 15.628 eV is shown in Figure S2. The plots show a similar intense,

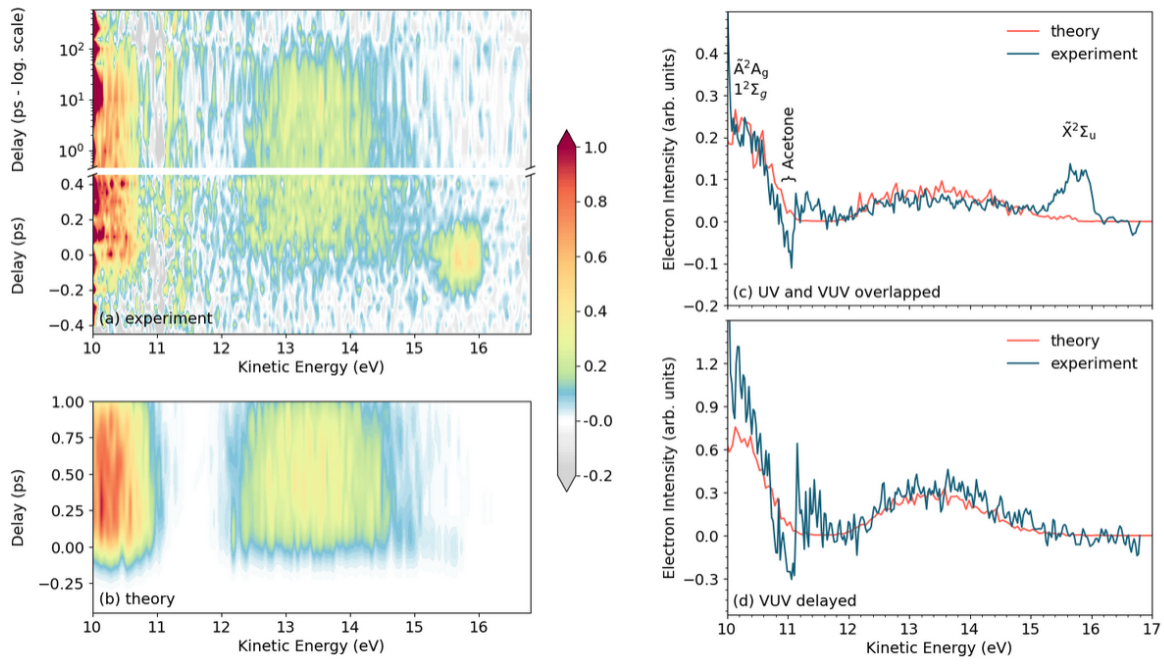

Figure 9. (a) A selected portion of the contour plot in Figure 6 showing the photoelectron intensities following UV + VUV ionization of C_2H_2 as a function of time delay and electron kinetic energy. The VUV probe corresponds to the fourth harmonic of the FEL at 20.838 eV. The plot is broken into two parts with a linear time axis at short delays and a log time axis at long delays. (b) The theoretical contour plot across the full-time interval of the calculations. (c) Cuts through the experimental and theoretical contour plots integrated for time delays of -0.2 to 0.2 ps corresponding to overlapped UV and VUV pulses. (d) Same as (c) but for time delays of time delays of 0.3 to 1 ps.

relatively sharp feature at an electron kinetic energy of ~15.6 eV in Figure 9a and at 10.4 eV in Figure S2 (i.e., shifted by 5.21 eV, the difference in photon energy), but only when the pump and probe pulses are overlapped in time. At longer delays, this feature disappears and is replaced by a broad continuous feature at kinetic energies between 11.8 and 14.8 eV in Figure 9a. The new feature decays very slowly on the timescale of the experiments, gradually disappearing at delays longer than ~100 ps. A third feature is observed at electron kinetic energies of ~10.2 – 10.9 eV in Figure 9a. The time dependence of this feature shows a sharp rise and fall like the 15.6 eV feature, but it also displays a second component that decays on a longer timescale like the 11.8 – 14.8 eV feature. The 10.2 – 10.9 eV feature likely extends to lower kinetic energies, but any such signal is buried under the signal from the much more intense single-photon ionization of the ground state.

Figure 9b shows the theoretical contour plot with a linear time axis for delays of -0.4 to 1.0 ps, the range of the trajectory calculations. To match the experimental time resolution, the spectrum was convolved with the pump-probe cross-correlation function, that is, with a temporal Gaussian function of 260 fs FWHM (see Ref. 71). The agreement between the experimental and theoretical plots is quite good, with the exception of the intense short-time feature between 15 and 16 eV in the experimental spectrum, which shows up only very weakly in the theoretical plot.

The changes in the pump-probe photoelectron spectra can be highlighted by comparing the behavior of different slices through the contour plots. Figure 9c and d show slices for different ranges of delays in the $h\nu_{vuv} = 20.838$ eV contour plots. The analogous slices for the $h\nu_{vuv} = 15.628$ eV contour plot are shown in Figure S3. Figures 9c and d also show the corresponding slices through the theoretical data, which have been scaled by an overall factor to match the experimental intensities. With the one exception discussed below, the agreement between the theoretical and experimental curves is generally excellent. Figure 9c shows the summed spectra for a range of delays in which the pump and probe pulses are temporally overlapped (delays of ~ -200 to +200 fs). The sharp rise in the signal below 10 eV electron kinetic energy is due to the onset of the single

VUV photon ionization of acetylene via the $\widetilde{X}\ ^2\Pi_u \leftarrow X\ ^1\Sigma_g^+$ transition. The oscillatory (and partially negative amplitude) feature near 11 eV electron kinetic energy is due to imperfect subtraction of the acetone impurity peak derived from single-photon ionization.

The structured feature in Figure 9c with kinetic energy between 15.2 and 16.1 eV corresponds to the UV + VUV two-photon ionization of acetylene at geometries close to the Franck-Condon region for excitation to the $\widetilde{A}\ ^1A_u$ state, to populate the $\widetilde{X}\ ^2\Pi_u$ state of the ion. Figure 9c shows a second feature with electron kinetic energy between 10 and 12 eV. This band is squeezed between two much more intense VUV-only features (ionization to the $X\ ^2\Pi_u$ ground state and ionization of an acetone impurity in the sample), limiting the detail in which it can be explored. The initial rise in the signal suggests that the short time signal arises from ionization of molecules with geometries local to the Franck-Condon region. Based purely on energetics, this feature could be assigned to UV + VUV two-photon ionization to populate either the $\widetilde{A}\ ^2\Sigma_g^+$ or $1\ ^2\Pi_g$ state of the cation through nonresonant ionization or resonant ionization via the $\widetilde{A}\ ^1A_u$ state. When the VUV and UV are overlapped in time, both the $\widetilde{A}\ ^2\Sigma_g^+$ or $1\ ^2\Pi_g$ may be strong but, as discussed below, when the VUV is delayed from the UV, intensity considerations suggest the latter assignment.

When the UV and VUV pulses are overlapped, and at very short delays, the resonant process is expected to produce a signal from the VUV ionization of the wavepacket formed by the UV pulse on the $\widetilde{A}\ ^1A_u$ surface and localized at the geometry of the neutral ground state. This process is expected to produce a photoelectron spectrum similar to that for single-photon ionization from the $X\ ^1\Sigma_g^+$ state, with a short progression in the $\widetilde{X}\ ^2\Pi_u$, ν_3^+, C≡C stretching vibration, and a somewhat more extended vibrational progression in the $\widetilde{A}\ ^2\Sigma_g^+$ state.[35] This signal will decay very rapidly (in a few fs) as the molecule moves away from the equilibrium geometry. This feature is very weak in the theoretical spectrum, which only considered the resonant (sequential) ionization process, suggesting that another mechanism may be contributing to its intensity. In particular, nonresonant two-photon UV + VUV ionization (i.e., non-sequential two-photon ionization) by off-resonant

components of the pulses is also possible when the pulses are temporally overlapped. This process is also expected to produce a photoelectron spectrum like that of the one-photon process. This process is not included in the theoretical calculations, and the intensity of the corresponding feature thus suggests that the nonresonant process may be making the dominant contribution to the process. However, distinguishing the relative contributions of the resonant and nonresonant processes is not straightforward, and it is possible that both contribute to the temporally overlapped signal. In principle, the resonant process will be shifted to slightly longer pump-pulse delay that is determined by the decay rate of the initially localized wavepacket. This delay is expected to be only a few fs, and is discussed in more detail below.

Figure 9d shows the summed spectra for delays of +0.3 ps to +1.0 ps, for which the two pulses are well-separated in time. The most striking difference from Figure 9c is the disappearance of the band with kinetic energy between 15.2 and 16.1 eV, and the rise of a strong broad continuum feature that extends from kinetic energy of ~12 eV to ~15.2 eV. This broad feature is only weakly present in Figure 9c. The new feature seems much more consistent with ionization out of high vibrational levels of the $\widetilde{A}\ ^1A_u$ state into the continuum of the $\widetilde{X}\ ^2\Pi_u$ state of the ion (i.e., the molecule has sampled a significant fraction of its available phase space). This feature is discussed in the context of the theoretical calculations below.

The behavior of the features in Figure S3 for the 15.628 eV probe is similar to that in Figure 9 for the 20.838 eV probe. A strong $\widetilde{X}\ ^2\Pi_u$ photoelectron signal like that in the single-photon spectrum is observed when the pulses are temporally overlapped, and this signal disappears when the probe is delayed. This feature is replaced in the delayed spectrum by a very broad feature, corresponding to $\widetilde{X}\ ^2\Pi_u$ ions with ~0.5 to 3.5 eV of internal energy. In Figure S3, the signal at the electron kinetic energies between 4.6 and 6.6 eV (corresponding to 9.8 to 11.8 eV kinetic energy in Figure 9) is present at both delays.

One point deserves mention here. The 200-nm pump pulse accesses vibrational levels of the neutral $\widetilde{A}\ ^1A_u$ state with ~0.97 eV of vibrational energy, while the peak in Figure 9d corresponds to the $\widetilde{X}\ ^2\Pi_u$ state ion with 2.4 eV of internal energy. Interestingly, while the dissociation energy of the $\widetilde{X}\ ^2\Pi_u$ state is 5.9571 ± 0.0009 eV,[30] the threshold for isomerization to the vinylidene $1\ ^2A_1$ state is predicted to be barrierless and less than 2 eV.[38,42] Thus, in principle, the highly excited vibrational levels populated in the $\widetilde{X}\ ^2\Pi_u$ state can undergo free isomerization to the vinylidene structure. Unfortunately, any signature of the vinylidene structure is likely smeared out by the large range of vibrational motion on both the $\widetilde{A}\ ^1A_u$ and $\widetilde{X}\ ^2\Pi_u$ surfaces, and the calculations for this process were not attempted.

We now consider the band in Figures 9c and 9d between 10 and 12 eV kinetic energy in more detail. The corresponding feature measured with the lower energy probe and plotted in Figure S3 has a similar appearance. The band is not well resolved, preventing a detailed assignment of the structure. Furthermore, there is some interference from the acetone impurity signal, and the full Franck-Condon envelope of the ionizing transition is cut off at ~10.0 eV electron kinetic energy by the extremely intense VUV-only signal. Nevertheless, the band shows a slow rise from an electron kinetic energy of 11.6 eV, corresponding to an energy 15.4 eV above the neutral $\widetilde{X}\ ^1\Sigma_g^+$ ground state if the process involves two-photon UV + VUV excitation. A second steeper rise is observed centered at a kinetic energy of 10.6 eV (16.4 eV above $\widetilde{X}\ ^1\Sigma_g^+$). This band is well-reproduced in the theoretical calculations of Figure 9. The qualitative arguments in the Introduction suggest that this band is due to UV + VUV photoionization to the $1\ ^1\Pi_g$ state, rather than to the $\widetilde{A}\ ^2\Sigma_g^+$ state. Specifically, when the UV and VUV pulses are overlapped in time, both the $\widetilde{A}\ ^2\Sigma_g^+$ and $1\ ^2\Pi_g$ states are expected, with the $\widetilde{A}\ ^2\Sigma_g^+$ state produced by the same nonresonant two-photon ionization process that accounts for the low vibrational levels of the $\widetilde{X}\ ^2\Pi_u$ state in Figure 9c, and with the $1\ ^2\Pi_g$ state produced with the two-step process via the $\widetilde{A}\ ^1A_u$ state. As discussed in the Introduction, however, with the delayed VUV pulse, the $\widetilde{A}\ ^2\Sigma_g^+$ state is only accessible via a two-electron transition driven by the probe pulse, and such transitions are expected

to be very weak. In contrast, VUV ionization out of the $1\pi_u$ orbital of the $\widetilde{A}\ ^1A_u$ state leads directly to the dominant configuration of the $1\ ^2\Pi_g$ state. The Dyson norms plotted in Figure 4 are consistent with this picture for the delayed ionization. The norms are extremely small for ionization to the $\widetilde{A}\ ^2\Sigma_g^+$ state for all geometries of the $\widetilde{A}\ ^1A_u$ state, while they are almost twice as large for ionization to the B_g component of the $1\ ^2\Pi_g$ state than for any other process from the $\widetilde{A}\ ^1A_u$ state. Systematic photoelectron studies with improved signal-to-noise ratio from a series of $\widetilde{A}\ ^1A_u$ vibrational levels are necessary to provide a more complete analysis of the $1\ ^2\Pi_g$ spectra.

Finally, two additional UV + VUV features are observed with electron kinetic energies below 9.4 eV in Figure 7. For kinetic energies between 7.5 and 8.2 eV, an increase in the signal is observed at time delays longer than ~30 ps, and is discussed in the next Section. Similarly, for electron kinetic energies between 5.6 and 7.0 eV, a time-dependent signal is observed that is similar to that of the signal at electron kinetic energies of 12.3 to 14.8eV. Neither of the features observed at kinetic energies below 9.4 eV are observed at the corresponding electron kinetic energies (i.e., below 4.2 eV) in spectra recorded with the 15.628 eV probe light. This result may be due in part to greater interference from large amplitude VUV_{only} signals and ringing in the latter spectra. Alternatively, this difference might suggest that these signals arise in connection with ionization processes that are only energetically allowed with the 20.838 eV light.

D. Time-Dependent Photoelectron Bands

The time dependence of the photoelectron band arising from nonresonant UV + VUV (fourth harmonic) two-photon ionization of He allows a determination of the instrument function and $\Delta t = 0$ for the pump-probe experiments. Figure 10a shows a plot of this time dependence, where the photoelectron signal was integrated for electron kinetic energies between 2.45 and 2.65 eV. Figure 10a also shows a fit of the data with a Gaussian lineshape function. The baseline of the peak is slightly asymmetric, reflecting the varying level of background signal from other processes, and was subtracted before the fit. The full width at half maximum (FWHM) of this peak is 289 ± 11

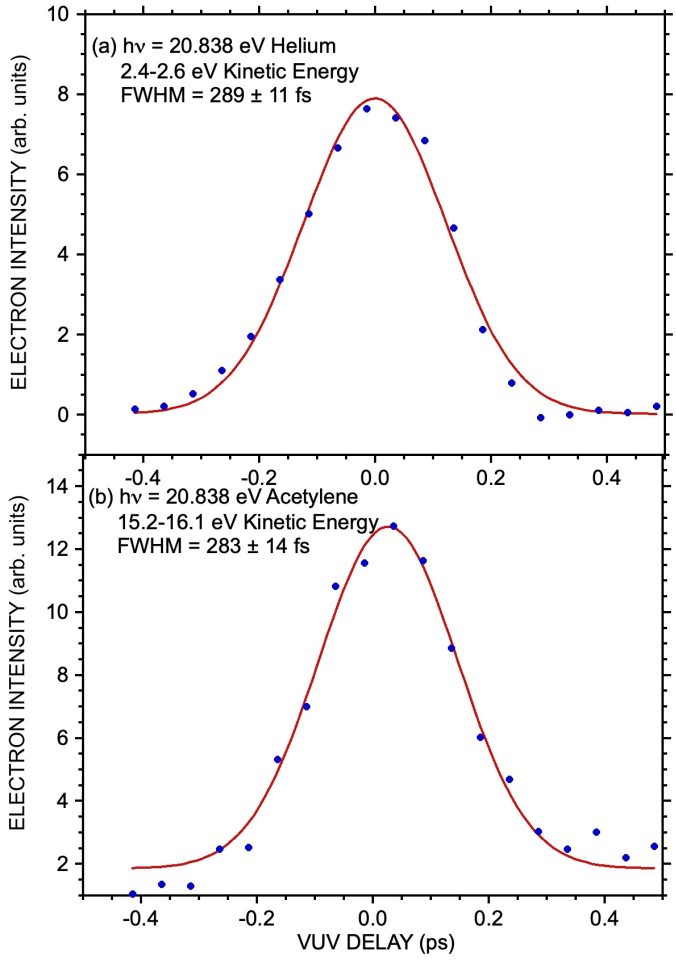

Figure 10. (a) The time dependence of the photoelectron signal recorded with the fourth harmonic probe for electron kinetic energies of 2.4 – 2.6 eV. This signal corresponds to the two-photon UV + VUV ionization of He. (b) The time dependence of the photoelectron signal recorded with the fourth harmonic probe for binding energies of 15.2 – 16.1 eV, corresponding to UV + VUV ionization to low vibrational levels of the $C_2H_2^+$ $^2\Pi_u$ state (see Figure 9c).

fs, slightly larger than the expected width of 261 fs calculated from the convolution of the estimated widths of the UV and VUV pulses. While the Gaussian lineshape does an excellent job at reproducing the experimental data, partial fits to the peak suggest that the risetime of the peak is slightly slower than the falltime. The center of the Gaussian peak was chosen as zero delay between the UV pump and the VUV probe.

Figure 10b shows the time dependence of the acetylene photoelectron band corresponding to the highest electron kinetic energy (15.1 to 16.2 eV) for ionization at 20.838 eV, using $\Delta t = 0$ from the He measurement. The corresponding data for the 15.628 eV probe are shown in Figure S4. As for the He peak, this band only occurs when the UV and VUV pulses are overlapped in time, and then rapidly disappears. As discussed in the previous section, this observation could arise from either resonant or nonresonant UV + VUV ionization of acetylene, the latter with either ordering of the two pulses. (Note that when the VUV photon comes first in the nonresonant process, the VUV + UV two-

photon process corresponds to above-threshold ionization. The complementary VUV – UV two-photon process is also possible, but the expected photoelectrons fall in the saturated region of photoelectrons from single-photon VUV photoionization to the $\tilde{A}\ ^2\Sigma_g^+$ state.) Gaussian fits of the data in Figures 10b and S4 yield similar results to those for the two-photon ionization of He, with FWHM of 283 ± 14 and 287 ± 10 fs for the 20.838 eV and 15.628 eV probes, respectively.

In principle, the position of the peak for the resonant process will be shifted to longer delay than for the nonresonant process, with the magnitude of the shift related to the decay time of the resonant feature. In the present case, the localized wavepacket is expected to decay in a few fs, spreading out across the accessible geometries in the intermediate state. Thus, the expected time delay is very small. The fitted position of the peak in Figure 10b is indeed shifted to longer delay than in Figure 10a by 26 ± 8 fs. This value corresponds to only one-half step in the time delay scan. Fitting the peak shape in Figure 10b by using the He response as the excitation function and fitting a decay constant yields a lifetime of 48 ± 8 fs (approximately one time step) for the molecule to move away from the Franck-Condon region of the pump transition. An improved signal-to-noise ratio and data on a finer time mesh are necessary to characterize this delay more fully.

Figure 11a shows the time dependence of the broad, 12.0 – 15.2 eV band in Figure 9c. The corresponding $h\nu_{VUV}$ = 15.628 eV data are shown in Figure S5. The time dependences in Figures 11 and S5 are similar to each other, and very different from those in Figure 10. Figure 11b shows an expanded portion of the data near zero pump-probe delay, along with the (scaled) integral of the fit to the He feature in Figure 10a. For resonant excitation to a very long-lived intermediate state, the rise of the ionization signal is expected to be proportional to the integral of the instrument response function. The close agreement between the acetylene curve and the integrated He signal is consistent with this expectation. As discussed in Section III.C, the long-delay behavior of Figure 11a reflects ionization from highly vibrationally excited levels of the $\tilde{A}\ ^1A_u$ state, along with the slow loss of the $\tilde{A}\ ^1A_u$ state population due to intersystem crossing and dissociation to H + C_2H.

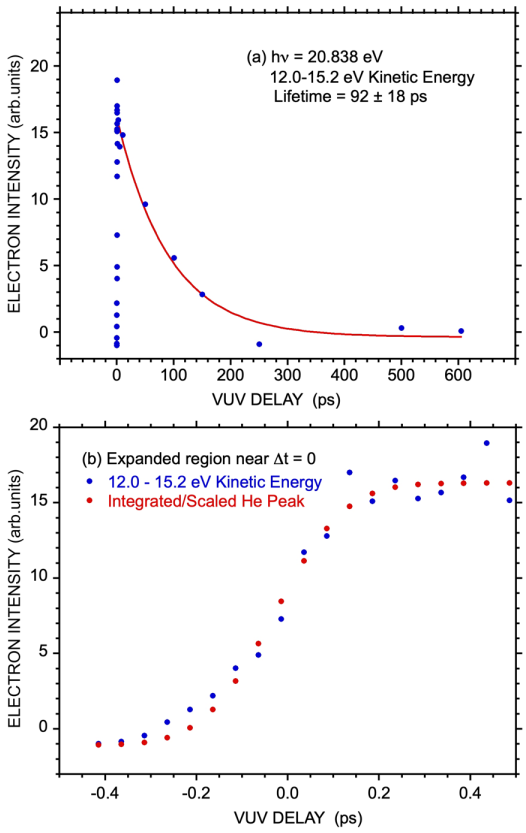

Figure 11. (a) The time dependence of the photoelectron signal recorded with the fourth harmonic probe for electron kinetic energies of 12.0 – 15.2 eV. (b) An expanded portion of the time-dependent signal near Δt = 0. Also shown is the integrated fit to the He signal in Figure 10a.

The data for the decay curves at longer times are rather noisy, but fitting the decay for delays between ~250 fs and 600 ps to an exponential form yields lifetimes of 72 ± 18 and 92 ± 18 ps for ionization at 15.628 and 20.838 eV, respectively. These values are consistent with the previously measured lifetimes of ~100 ps for intersystem crossing from $\tilde{A}\ ^1A_u$ state levels near the dissociation limit, although shorter lifetimes of ~25 ps have been measured at slightly higher energies (6.274 eV).[32]

Figure 12 shows the time dependence of the band with electron kinetic energy between 10.2 eV and 10.7 eV shown in Figure 9. The corresponding data for $h\nu_{VUV}$ = 15.628 eV are shown in Figure S6. This band corresponds to ionization populating the 1 $^2\Pi_g$ and $\tilde{A}\ ^2\Sigma_g^+$ states of the ion. Both sets of data show a strong prompt peak that is similar to that observed in Figure 10b, along with a slower process with a decay time similar to that in Figures 11 and S5. As in Figure 10, the prompt/fast feature is likely due to either resonant or nonresonant two-photon ionization to the $\tilde{A}\ ^2\Sigma_g^+$ and 1 $^2\Pi_g$ states. The transition to the $\tilde{A}\ ^2\Sigma_g^+$ state is expected to contribute more strongly than the 1 $^2\Pi_g$ state at short times due to the nonresonant ionization process. However, when the probe and pump are separated in time, the 1 $^2\Pi_g$ state is expected to make the dominant contribution based on the corresponding Dyson norms. While the appearance

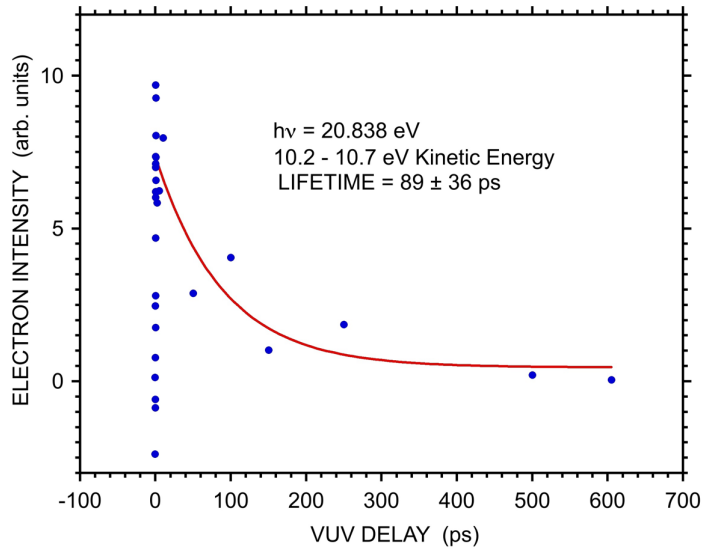

Figure 12. The time dependence of the photoelectron signal recorded with the fourth harmonic (20.838 eV) probe for electron kinetic energies of 10.2 – 10.7 eV.

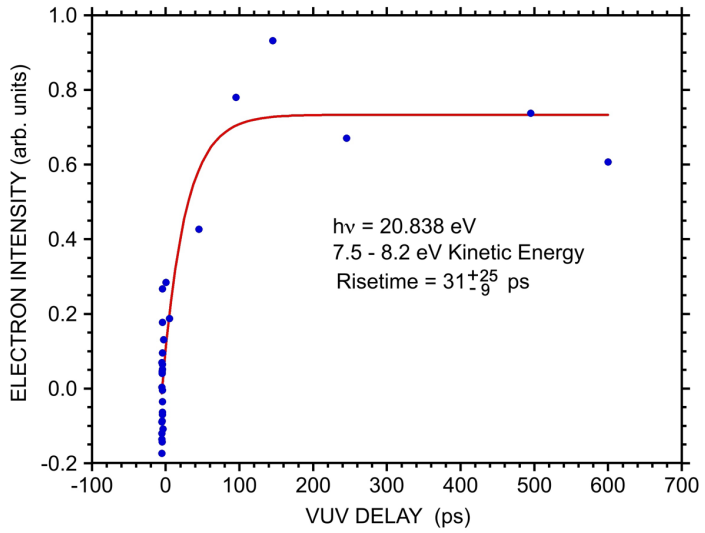

Figure 13. The time dependence of the photoelectron signal recorded with the fourth harmonic (20.838 eV) probe for electron kinetic energies of 7.5 – 8.2 eV. The fit to an exponential rise time is also shown.

of this feature in the photoelectron spectra of Figures 9 and S3 does change somewhat in the overlapped vs. delayed VUV spectra, the data quality is not sufficient to clearly distinguish and separate the contributions from the two ionization processes.

Figure 13 shows the time dependence of the band in Figure 7 with kinetic energy between 7.5 eV and 8.2 eV. An exponential fit to the rise time gives a value of 31^{+25}_{-9} ps. The behavior of this feature suggests that it may come from the ionization of triplet acetylene or of C_2H fragments, but the energetics suggest this would involve highly excited vibrational levels and/or excited electronic states of the corresponding cations. Although the value of the rise time is somewhat faster than the decay times observed for the other features, the error bars are relatively large.

IV. CONCLUSIONS

We have presented new UV + VUV time-resolved mass spectra and photoelectron spectra for high vibrational levels of the $\widetilde{A}\ ^1A_u$ state of acetylene. The mass spectra show evidence for dissociative ionization by the UV + VUV pulses, and by the VUV pulses alone. The mass spectra also show evidence for the photoionization of neutral fragments, and for the photodissociation of the parent ion. The photoelectron spectra recorded with the two pulses overlapped may have contributions from both nonresonant two-photon ionization and resonant ionization of a highly localized $\widetilde{A}\ ^1A_u$ wavepacket. The delayed signal reflects the ionization of high vibrational levels of the $\widetilde{A}\ ^1A_u$ state populated by the UV pump at 6.199 eV. The decay of this signal occurs on a timescale consistent with previously measured intersystem crossing rates.[32] The delayed ionization process leads to the population of a very broad distribution of vibrational levels in the $C_2H_2^+$ $\widetilde{X}\ ^2\Pi_u$ state. In addition, the delayed photoelectron spectra also show a strong feature that can be assigned to the previously unobserved $C_2H_2^+$ $1\ ^2\Pi_g$ state, which corresponds to a two-hole, one-particle configuration in the ion that is not accessible via a pure single-photon, electric-dipole process. The present experiments and interpretation are supported by theoretical calculations of the photoelectron spectra and their time dependence for the $\widetilde{A}\ ^1A_u$ state. In particular, the calculations confirm a strong ionization transition from the $\widetilde{A}\ ^1A_u$ state to the $1\ ^2\Pi_g$ state, along with a very weak transition from the $\widetilde{A}\ ^1A_u$ state to the $\widetilde{A}\ ^2\Sigma_g^+$ state.

While only weakly accessible (and previously unobserved) in single-photon ionization studies near threshold,[39] two-hole, one-particle states like $C_2H_2^+$ $1\ ^2\Pi_g$ are often populated through spectator decay in resonant Auger-Meitner electron spectra.[43,44] Direct access of such states through resonant two-photon excitation combined with high-resolution photoelectron spectroscopy, is expected to provide a powerful tool for the characterization of these states.

V. ACKNOWLEDGEMENTS

We are grateful to the FERMI staff for running the facility and providing beamtime under Project No. 20199044. RSM would like to thank the EPSRC (EP/X027635/1) and Leverhulme (RPG-2021-257) trust for financial support. WOR thanks the STFC UK XFEL hub for physical sciences and the University of Southampton for a studentship. The work of TP and ND has been financially supported by the Croatian Science Foundation (HRZZ) (grant number IP-2022-10-4658) The work of RF and RJS has been financially supported by the Swedish Research Council (VR) (grant numbers 2018-03731 and 2023-03464) and the Knut and Alice Wallenberg Foundation (grant number 2017.0104), Sweden. DMPH is grateful to the Science and Technology Facilities Council (United Kingdom) for financial support. STP is supported by the U.S. Department of Energy, Office of Science, Office of Basic Energy Sciences, Division of Chemical Sciences, Geosciences, and Biosciences under contract No. DE-AC02-06CH11357.

REFERENCE

1. A. Stolow, A. E. Bragg, and D. M. Neumark, Femtosecond time-resolved photoelectron spectroscopy, Chem. Rev. **104**, 1719-1757 (2004).
2. T. Suzuki, Femtosecond time-resolved photoelectron imaging, Annu. Rev. Phys. Chem. **57**, 555-592 (2006).
3. M. S. Schuurman and V. Blanchet, Time-resolved photoelectron spectroscopy: the continuing evolution of a mature technique, Phys. Chem. Chem. Phys. **24**, 20012 (2022).
4. J. Nishitani, C. W. West, C. Higashimura, and T. Suzuki, Time-resolved photoelectron spectroscopy of polyatomic molecules using 42-nm vacuum ultraviolet laser based on high harmonics generation, Chem. Phys. Lett. **684**, 397-401 (2017).
5. R. Uenishi, A. Boyer, S. Karashima, A. Humeniuk, and T. Suzuki, Signatures of conical intersections in extreme ultraviolet photoelectron spectra of furan measured with 15 fs time resolution, J. Phys. Chem. Lett. **15**, 2222-2227 (2024).
6. S. Y. Liu, Y. Ogi, T. Fujii, K. Nishisawa, T. Horio, T. Mizuno, H. Kohguchi, M. Nagasono, T. Togashi, K. Tono, M. Yabashi, Y. Senba, H. Ohashi, H. Kimura, T. Ishikawa, and T. Suzuki, Time-resolved photoelectron imaging using a femtosecond UV laser and a VUV free-electron laser, Phys. Rev. A **81**, 031403(R) (2010).
7. P. Johnsson, A. Rouzée, W. Siu, Y. Huismans. F. Lépine, T. Marchenko, S. Düsterer, F. Tavella, N. Stojanovic, A. Azima, R. Treusch, M. F. Kling, and M. J. J. Vrakking, Field-free molecular alignment probed by the free electron laser at Hamburg (FLASH), J. Phys. B **42**, 134017 (2009).
8. R.J. Squibb, M. Sapunar, A. Ponzi, R. Richter, A. Kivimäki, O. Plekan, P. Finetti, N. Sisourat, V. Zhaunerchyk, T. Marchenko, L. Journel, R. Guillemin, R. Cucini, M. Coreno, C. Grazioli, M. Di Fraia, C. Callegari, K.C. Prince, P. Decleva, M. Simon, J.H.D. Eland, N. Došlić, R. Feifel, and M.N. Piancastelli, Acetylacetone photodynamics at a seeded free-electron laser, Nat. Commun. **9**, 63 (2018).

9. O. Gessner and M. Gühr, Monitoring ultrafast chemical dynamics by time-domain x-ray photo- and Auger-electron spectroscopy, Acc. Chem. Res. **49**, 138-145 (2016).
10. A. Al-Haddad, S. Oberli, J. González-Vázquez, M. Bucher, F. Doumy, P. Ho, J. Kryzywinski, T. J. Lane, A. Lutman, A. Marinelli, T. J. Maxwell, S. Moeller, S. T. Pratt, D. Ray, R. Shepard, S. H. Southworth, A. Vázquez-Mayagoitia, P. Walter, L. Young, A. Picón, and C. Bostedt, Observation of site-selective chemical bond changes via ultrafast chemical shifts, Nat. Commun. **13**, 7170 (2022).
11. C. K. Ingold and G. W. King, Excited states of acetylene. Parts I-V. J. Chem. Soc. 2702-2755 (1953).
12. K. K. Innes, Analysis of the near ultraviolet absorption spectrum of acetylene, J. Chem. Phys. 22, 863-876 (1954).
13. J. C. Van Craen, M. Herman, and R. Colin, The $\tilde{A}$-$\tilde{X}$ band of acetylene: bands of the short-wavelength region, J. Mol. Spectrosc. **119**, 137-143 (1986).
14. A. Haijima, M. Fujii, and M. Ito, Predissociation of the acetylene $\tilde{\mathbf{A}}\ ^1A_u$ state and its mechanism, J. Chem. Phys. 92, 959-968 (1990).
15. T. Suzuki, Y. Shi, and H. Kohguchi, Detection of metastable triplet acetylene produced by intersystem crossing from the $\tilde{\mathbf{A}}$ (^1A_u) state, J. Chem. Phys. **106**, 5292-5295 (1997).
16. R. L. Thom, B. M. Wong, R. W. Field, and J. F. Stanton, Studies of intersystem crossing dynamics in acetylene, J. Chem. Phys. **126**, 184307 (2007).
17. A. J. Merer, A. H. Steeves, J. H. Baraban, H. A. Bechtel, and R. W. Field, *Cis-trans* isomerization in the S_1 state of acetylene: Identification of cis-well vibrational levels, J. Chem. Phys. **134**, 244310 (2011).

18. D. H. Mordaunt and M. N. R. Ashfold, Near ultraviolet photolysis of C_2H_2: A precise determination of *D*(HCC−H), J. Chem. Phys. **101**, 2630-2631(1994).

19. N. Hashimoto and T. Suzuki, Energy and state dependence in the quenching and predissociation of C_2H_2, J. Chem. Phys. **104**, 6070-6073 (1996).

20. S. H. S. Wilson, C. L. Reed, D. H. Mordaunt, M. N. R. Ashfold, and M. Kawasaki, Near-threshold photodissociation of C_2H_2, C_2HD, and C_2D_2 studied by H(D) atom photofragment translational spectroscopy, Bull. Chem. Soc. Jpn, **69**, 71-76 (1996).

21. N. Hashimoto, N. Yonekura, and T. Suzuki, Pump-probe measurements of the predissociation reaction time of C_2H_2 from the $\tilde{\mathbf{A}}$ (^1A_u) state, Chem. Phys. Lett. **264**, 545-550 (1997).

22. D. H. Mordaunt, M. N. R. Ashfold, R. N. Dixon, P. Löffler, L. Schneider, and K. H. Welge, Near threshold photodissociation of acetylene, J. Chem. Phys. **108**, 519-526 (1998).

23. Y. Shi and T. Suzuki, Formation of metastable triplet acetylene from the $\tilde{\mathbf{A}}$ (^1A_u) state near the dissociation threshold, J. Phys. Chem. A **102**, 7414-7419 (1998).

24. T. Suzuki and N. Hashimoto, Predissociation of acetylene from the $\tilde{\mathbf{A}}$ ^1A_u state studied by absorption, laser-induced fluorescence, and H-atom action spectroscopies, J. Chem. Phys. **110**, 2042-2050 (1999).

25. M. Perić, R. J. Buenker, and S. D. Peyerimhoff, Theoretical study of the U.V. spectrum of acetylene, Mol. Phys. **53**, 1177-1193 (1984).

26. J. F. Stanton, C. M. Huang, and P. G. Szalay, Stationary points on the S_1 potential energy surface of C_2H_2, J. Chem. Phys. **101**, 356-365 (1994).

27. Q. Cui, K. Morokuma, and J. F. Stanton, Ab initio MO studies on the photodissociation of C_2H_2 from the $S_1(^1A_u)$ state. Non-adiabatic effects and S-T interaction, Chem. Phys. Lett. **263**, 46-53 (1996).

28. Q. Cui and K. Morokuma, Ab initio MO studies on the photodissociation of C_2H_2 from the S_1 (^1A_u) state. II. Mechanism involving triplet states, Chem. Phys. Lett., **272**, 319-327 (1997).
29. E. Ventura, M. Dallos, and H. Lischka, The valence excited states T_1-T_4 and S_1-S_2 of acetylene: A high-level MR-CISD and MR-AQCC investigation of stationary points, potential energy surfaces, and surface crossings, J. Chem. Phys. **118**, 1702-1713 (2003).
30. B. Ruscic and D. H. Bross, Active Thermochemical Tables (ATcT) values based on ver. 1.122v of the Thermochemical Network, Argonne National Laboratory, Lemont, Illinois 2022; available at ATcT.anl.gov.
31. E. N. Sharp-Williams, M. A. Roberts, and D. J. Nesbitt, High resolution slit-jet infrared spectroscopy of ethynyl radical: ^2P – $^2S^+$ vibronic bands with sub-Doppler resolution, J. Chem. Phys. 134, 064314 (2011).
32. N. Yamakita, S. Iwamoto, and S. Tsuchiya, Predissociation of excited acetylene in the $\widetilde{\mathbf{A}}$ ^1A_u state around the adiabatic dissociation threshold as studied by LIF and H-atom action spectroscopy, J. Phys. Chem. A **107**, 2597-2605 (2003).
33. E. Allaria, L. Badano, S. Bassanese, F. Capotondi, D. Castronovo, P. Cinquegrana, M. B. Danailov, G. D'Auria, A. Demidovich, R. De Monte, G. De Ninno, S. Di Mitri, B. Diviacco, W. M. Fawley, M. Ferianis, E. Ferrari, G. Gaio, D. Gauthier, L. Giannessi, F. Iazzourene, G. Kurdi, N. Mahne, I. Nikolov, F. Parmigiani, G. Penco, L. Raimondi, P. Rebernik, F. Rossi, E. Roussel, C. Scafuri, C. Serpico, P. Sigalotti, C. Spezzani, M. Svandrlik, C. Svetina, M. Trovó, M. Veronese, D. Zangrando, and M. Zangrando, The FERMI free-electron lasers, J. Synch. Rad. **22**, 485-491 (2015).
34. K. Kimura, S. Kasumata, Y. Achiba, T. Yamazaki, and S. Iwata, *Handbook of He I Photoelectron Spectra of Fundamental Organic Molecules* (Halsted Press, New York, 1981).

35. J. E. Reutt, L. S. Wang, J. E. Pollard, D. J. Trevor, Y. T. Lee, and D. A. Shirley, Photoelectron spectroscopy and inferred femtosecond intramolecular dynamics of $C_2H_2^+$ and $C_2D_2^+$, J. Chem. Phys. 84, 3022-3031 (1986).

36. S. T. Pratt. P. M. Dehmer, and J. L. Dehmer, Photoelectron spectroscopy from the A ^1A_u state of acetylene – the bending vibrations of $C_2H_2^+$ X ^2P_u, J. Chem. Phys. **95**, 6238-6248 (1991).

37. P. Hockett, A. K. King, I. Powis, and K. L. Reid, Complete determination of the photoionization dynamics of a polyatomic molecule: I: Experimental photoelectron angular distributions from $\widetilde{A}$ ^1A_u acetylene, J. Chem. Phys. **127**, 154307 (2007).

38. P. Rosmus, P. Botschwina, and J. P. Maier, On the ionic states of vinylidene and acetylene, Chem. Phys. Lett. **84**, 71-76 (1981).

39. L. Cederbaum, W. Domcke, J. Schirmer, and W. von Niessen, Correlation effects in the ionization of molecules: breakdown of the molecular orbital picture, Adv. Chem. Phys. **65**, 115-159 (1986).

40. W. P. Kraemer and W. Koch, A CASSCF-CI study of the ground and low-lying excited electronic states of $C_2H_2^+$, Chem. Phys. Lett. **212**, 631-636 (1993).

41. G. Chambaud R. Van den Boom, and P. Rosmus, On the mechanism of energy redistribution in the $\widetilde{A}$ $^2\Sigma_g^+$ state of the $HCCH^+$ ion, Chem. Phys. Lett. **247**, 79-84 (1995).

42. S. Boyé-Péronne, D. Gauyacq, and J. Liévin, Vinylidene-acetylene cation isomerization investigated by large scale *ab initio* calculations, J. Chem. Phys. **126**, 214305 (2006).

43. V. Schmidt, Electron Spectrometry of Atoms using Synchrotron Radiation (Cambridge University Press, Cambridge, U.K., 1997).

44. G. B. Armen, H. Aksela, T. Åberg, and S. Aksela, The resonant Auger effect, J. Phys. B **33**, R49-R92 (2000).

45. E. Allaria, L. Badano, S. Bassanese, F. Capotondi, D. Castronovo, P. Cinquegrana, M. B. Danailov, G. D'Auria, A. Demidovich, R. De Monte, G. De Ninno, S. Di Mitri, B. Diviacco, W. M. Fawley, M. Ferianis, E. Ferrari, G. Gaio, D. Gauthier, L. Giannessi, F. Iazzourene, G. Kurdi, N. Mahne, I. Nikolov, F. Parmigiani, G. Penco, L. Raimondi, P. Rebernik, F. Rossi, E. Roussel, C. Scafuri, C. Serpico, P. Sigalotti, C. Spezzani, M. Svandrlik, C. Svetina, M. Trovó, M. Veronese, D. Zangrando, and M. Zangrando, The FERMI free-electron lasers, J. Synch. Rad. **22**, 485-491 (2015).
46. C. Svetina, C. Grazioli, N. Mahne, L. Raimondi, C. Fava, M. Zangrando, S. Gerusina, M. Alagia, L. Avaldi, G. Cautero, M. de Simone, M. Devetta, M. Di Fraia, M. Drabbels, V. Feyer, P. Finetti, R. Katzy, A. Kivimäki, V. Lyamayev, T. Mazza, A. Moise, T. Möller, P. O'Keeffe, Y. Ovcharenko, Paolo Piseri, O. Plekan, K. C. Prince, R. Sergo, F. Stienkemeier, S. Stranges, M. Coreno, and C. Callegari, The Low Density Matter (LDM) beamline at FERMI: optical layout and first commissioning, J. Synch. Rad. **22**, 538-543 (2015).
47. V. Lyamayev, Y. Ovcharenko, R. Katzy, M. Devetta, L. Bruder, A. LaForge, M. Mudrich, U. Person, F. Stienkemeier, M. Krikunova, T. Möller, P. Piseri, L. Avaldi, M. Coreno, P. O'Keeffe, P. Bolognesi, M. Alagia, A. Kivimäki, M. Di Fraia, N. B Brauer, M. Drabbels, T. Mazza, S. Stranges, P. Finetti, C. Grazioli, O. Plekan, R. Richter, K. C. Prince, and C. Callegari, A modular end-station for atomic, molecular, and cluster science at the low density matter beamline of FERMI@Elettra, J. Phys. B: At. Mol. Opt. Phys. **46**, 1-8 (2013).
48. C. Svetina, D. Cocco, N. Mahne, L. Raimondi, E. Ferrari and M. Zangrando. PRESTO, the on-line photon energy spectrometer at FERMI: design, features and commissioning results, J. Synchrotron Rad. **23**, 35-42 (2016).
49. P. Finetti, A. Demidovich, O. Plekan, M. Di Fraia, R. Cucini, C. Callegari, P. Cinquegrana, P. Sigalotti, R. Ivanov, M. B. Danailov, Claudio Fava, G. De Ninno, M. Coreno, C. Grazioli,

R. Feifel, R. J. Squibb, T. Mazza, M. Meyer, and K. C. Prince, Optical setup for two-colour experiments at the low-density matter beamline of FERMI, J. Opt. **19**, 114010 (2017).

50. The Supplemental Material can be found at:

51. M. Zangrando, C. Fava, S. Gerusina, R. Gobessi, N. Mahne, E. Mazzucco, L. Raimondi, L. Rumiz, and C. Svetina, The experience of the FERMI@Elettra photon beam transport and diagnostics system (PADReS) during three years of continuous support of machine and user experiments: achievements, lessons learned, and future upgrades, in *X-Ray Free-Electron Lasers: Beam Diagnostics, Beamline Instrumentation, and Applications II*, **9210**, 921003 (2014), DOI: 10.1117/12.2062980.

52. NIST Chemistry WebBook, NIST Standard Reference Database Number 69, Eds. P.J. Linstrom and W.G. Mallard, available at: https://webbook.nist.gov/chemistry/

53. P. Rupper and F. Merkt, Intense narrow-bandwidth extreme ultraviolet laser system tunable up to 20 eV, Rev. Sci. Instrum. **75**, 613-622 (2004).

54. R. T. Wiedmann, L. Goodman, and M. G. White, Two-color zero kinetic energy – pulsed field ionization spectroscopy of the acetone n-radical cation: the a_2 torsional vibration, Chem. Phys. Lett., **293**, 391-396 (1998).

55. T. Shiozaki, W. Gyorffy, P. Celani, H. -J. Werner, Extended multi-state complete active space second-order perturbation theory: energy and nuclear gradients. *J. Chem. Phys.* **135,** 081106 (2011).

56. T. Shiozaki, BAGEL: Brilliantly Advanced General Electronic-structure Library, Wiley Interdisciplinary Reviews: Computational Molecular Science 2018, 8, e1331.

57. D. Rappoport and F. Furche, Property-optimized Gaussian basis sets for molecular response calculations, J. Chem. Phys. 133, 134105 (2010).

58. B. Vlaisavljevich and T. Shiozaki, Nuclear Energy Gradients for Internally Contracted Complete Active Space Second-Order Perturbation Theory: Multistate Extensions, Journal of Chemical Theory and Computation **12**, 3781–3787 (2016).

59. J. W. Park and T. Shiozaki, Analytical derivative coupling for multistate CASPT2 theory, *J. Chem. Theory Comput.* **13,** 2561–2570 (2017).

60. Y. J. Yan, L. E. Fried, and S. Mukamel, Ultrafast Pump-Probe Spectroscopy: Femtosecond Dynamics in Liouville Space. *J. Phys. Chem.* **93,** 8149–8162 (1989).

61. Y. J. Yan and S. Mukamel, Femtosecond pump-probe spectroscopy of polyatomic molecules in condensed phases. *Phys. Rev. A* **14,** 6485–6504 (1990).

62. M. F. Gelin, X. Huang, W. Xie, L. Chen, N. Došlić, and W. Domcke, Ab initio surface-hopping simulation of femtosecond transient absorption pump-probe signals of nonadiabatic excited state dynamics using the doorway-window representation. *J. Chem. Theory Comput.* **17,** 2394–2408 (2021).

63. T. Piteša, M. Sapunar A. Ponzi, M. F. Gelin, N. Došlić, and W. Domcke, A combined surface-hopping, Dyson orbital and B-spline approach for the computation of time-resolved photoelectron spectroscopy signals: the internal conversion in pyrazine. *J. Chem. Theory Comput.* **17,** 5098–5109 (2021).

64. J. C. Tully, Molecular dynamics with electronic transitions. *J. Chem. Phys.* **93,** 1061–1071 (1990).

65. T. Shiozaki, BAGEL: Brilliantly Advanced General Electronic structure Library. http://www.nubakery.org under the GNU General Public License.

66. T. Piteša, M. Sapunar A. Ponzi, M. F. Gelin, N. Došlić, and W. Domcke, A combined surface-hopping, Dyson orbital and B-spline approach for the computation of time-resolved

photoelectron spectroscopy signals: the internal conversion in pyrazine. J. Chem. Theory Comput. **17**, 5098–5109 (2021).

67. O. Travnikova, T. Piteša, A. Ponzi, M. Sapunar, R. J. Squibb, R. Richter, P. Finetti, M. Di Fraia, A. De Fanis, N. Mahne, M. Manfredda, V. Zhaunerchyk, T. Marchenko, R. Guillemin, L. Journel, K. C. Prince, C. Callegari, M. Simon, R. Feifel, P. Decleva, N. Došlić, and M. N. Piancastelli, Photochemical Ring-Opening Reaction of 1,3-Cyclohexadiene: Identifying the True Reactive State, J. Am. Chem. Soc. **144**, 21878−21886 (2022)
68. M. Perić, R. J. Buenker, and S. D. Peyerimhoff, Theoretical study of the U.V. spectrum of acetylene, Mol. Phys. **53**, 1177-1193 (1984).
69. M. Perić, B. Engels, and M. Hanrath, Ab initio study of the electronic spectrum of $C_2H_2^+$. I. Vertical spectrum and angular potential curves. Chem. Phys. **238**, 33-46 (1998).
70. R. A. Mackie, S. W. J. Scully, A. M. Sands, R. Browning, K. F. Dunn, and C. J. Latimer, A photoionization mass spectrometric study of acetylene and ethylene in the VUV spectral region, Int. J. Mass Spectrom. **223-224**, 67-79 (2003)
71. V. Bonačić-Koutecký and R. Mitrić, Theoretical Exploration of Ultrafast Dynamics in Atomic Clusters: Analysis and Control. *Chem. Rev.* **105,** 11–65 (2005).